

Scour Pool Incision in Bedrock Canyons

by

Zhihao Cao

B.Sc., Simon Fraser University, 2015

Thesis Submitted in Partial Fulfillment of the
Requirements for the Degree of
Master of Science

in the
Department of Geography
Faculty of Environment

© Zhihao Cao 2018

SIMON FRASER UNIVERSITY

Spring 2018

Copyright in this work rests with the author. Please ensure that any reproduction or re-use is done in accordance with the relevant national copyright legislation.

Approval

Name: **Zhihao Cao**

Degree: **Master of Science**

Title: **Scour Pool Incision in Bedrock Canyons**

Examining Committee: **Chair: Nicolas Blomley**
Professor

Dr. Jeremy Venditti
Senior Supervisor
Professor

Dr. Michael Church
Supervisor
Professor Emeritus
Department of Geography
University of British Columbia

Dr. Eva Kwoil
Supervisor
Assistant Professor
Department of Geography
University of Victoria

Dr. Brett Eaton
External Examiner
Associate Professor
Department of Geography
University of British Columbia

Date Defended/Approved: April 30, 2018

Abstract

A flume experiment was conducted to investigate the effect of lateral constrictions on the initiation and evolution of scour pools in bedrock canyons. Results show that lateral constriction can initiate the formation of a scour pool. Deceleration of the flow upstream of the constricted canyon promotes alluviation, while flow acceleration through the canyon prevents a permanent sediment cover from developing. The elevation difference upstream and through the canyon causes flow and sediment to plunge towards the bed, enhancing scouring. The erosion rate was controlled by sediment size and presence of alluvial cover. Scour pools reach equilibrium morphology for a given constant discharge and sediment supply by cutting a slot, which then gets deep enough to maintain a permanent alluvial cover, protecting the bed from further vertical erosion and promoting lateral erosion. Shear stress calculated from the near-bed velocity gradient and Reynolds shear stresses are counterintuitively large in alluviated areas and low in places where the bed is clear of sediment. This highlights a general problem with using shear stress as a predictor of alluviation and rock erosion patterns in highly non-uniform flows. However, changes in near-bed velocity had strong correlations with alluviation patterns and erosion rate, suggesting near-bed velocity may be a more practical way to calculate rock erosion rates in non-uniform flows.

Keywords: scour pool; bedrock canyon; bedrock incision; lateral constriction; bedrock river

Table of Contents

Approval	ii
Abstract	iii
Table of Contents	iv
List of Tables	vi
List of Figures	vii
Chapter 1. Introduction	1
Chapter 2. Methods.....	5
2.1. Experimental setup	5
2.2. Experimental procedures	7
2.3. Observations	8
2.4. Data analysis.....	10
2.4.1. Calculating erosion volume and rate	10
2.4.2. Shear stress calculations.....	11
2.4.3. Entrainment threshold calculations	12
Chapter 3. Erosion Pattern, Rate and Volume.....	13
3.1. Bed elevation and water surface elevation	13
3.2. Erosion pattern.....	16
3.3. Intermittent alluviation cycles.....	20
3.4. Local erosion volumes and rates	20
3.5. Cumulative erosion volume and rates	23
Chapter 4. Patterns of Velocity and Shear Stress	26
4.1. Comparison of the shear stress estimation methods.....	26
4.2. Velocity and shear stress distribution prior to sediment feed	27
4.3. Velocity and shear stress distribution after alluviation and erosion	30
4.4. Velocity and shear stress relative to thresholds	33
Chapter 5. Discussion	34
5.1. Observed and expected erosion pattern	34
5.2. Influence of sediment on equilibrium morphology.....	35
5.3. Plunging flow and vertical velocity	37
5.4. Relations between velocity, shear stress and erosion patterns.....	38
Chapter 6. Conclusion.....	40
References.....	41
Appendix A. Photograph of flume setup.....	45
Appendix B. Photograph of erosion pattern with sediment.....	46

Appendix C. Photograph of short-term alluviation pattern..... 47
Appendix D. Foam slices showing cross-section of canyon section 48

List of Tables

Table 1.	Summary of initial flume conditions for all runs.....	14
Table 2.	Summary of flume conditions at eroded stage for completed runs.	14
Table 3.	Cumulative erosion for the entire canyon reach, derived from 2 methods.	25

List of Figures

Figure 1.	Geometry of Chimney Creek Canyon, Fraser River, showing long profile of the canyon with entrance and exit reaches. Water surface elevation at estimated discharge of 835 m ³ /s in September 2009.....	1
Figure 2.	Schematic of the flume setup showing lateral constriction in the canyon reach of the channel (not to scale).	5
Figure 3.	Initial water surface elevation, bed elevation and reference elevation for Run 1. Numbers 1-5 indicate the location of the 5 ADV velocity profiles. .	9
Figure 4.	Change of bed elevation and water surface elevation over time for a) Run 1, b) Run 2, c) Run 4 and d) Run 5. Legend shows run time in hours for each measurement, dashed lines indicate initial elevations.	16
Figure 5.	Erosion pattern from 12 hour to 100 hour for Run 5 showing the initiation and development of the primary pool and the secondary pool, within the constricted canyon. Panels a) and b) are the same images with and without the pool outlined using dashed lines.....	17
Figure 6.	Depth of the pool formation over time for a) Run 1, b) Run 2, c) Run 4 and d) Run 5.....	18
Figure 7.	Foam slices showing cross section of the pool formation with reference to where each slice was taken from along the canyon reach for a) Run 1, b) Run 2, c) Run 4 and d) Run 5. Number is the bottom right of slices indicates distance from the canyon entrance.....	19
Figure 8.	Illustration of a typical alluviation cycle that occurs during the experiment based on photos taken during the run, the channel bed constantly transitions between low sediment cover to high sediment cover, with varying degrees in each cycle.	21
Figure 9.	Volume of foam eroded over time at 6 locations within the pool formation a) Run 1, b) Run 2, c) Run 4 and d) Run 5.	21
Figure 10.	Local erosion rate over time at 6 locations within the pool for a) Run 1, b) Run 2, c) Run 4 and d) Run 5.....	22
Figure 11.	Final volume of foam material eroded at each location within the canyon reach, including 10 cm upstream of the canyon entrance shown as negative values, for a) Run 1, b) Run 2, c) Run 4 and d) Run 5.	24
Figure 12.	Comparison of shear stress calculated using the full profile method with a) the 2 point profile method and b) Reynolds stress method. Regressions are corrected to reduced major axis functional relations using Mark and Church (1977).	26
Figure 13.	Initial velocity profile at 5 locations (Figure 3) for all runs, before sediment was added to the flume, left column uses linear scale for relative depth on y-axis, right column uses logarithmic scale for relative depth on y-axis..	28
Figure 14.	Mean velocity along the channel measured at $z/d = 0.4$ during the a) initial stage, b) alluviated stage and c) eroded stage.	29
Figure 15.	Near-bed velocity measured at 6mm above the bed during the a) initial stage, b) alluviated stage and c) eroded stage.	29

Figure 16.	Shear stress derived from the 2 point profiles (solid points) and near-bed Reynolds stress (hollow points) along the channel measured during the a) initial stage, b) alluviated stage and c) eroded stage.	30
Figure 17.	Alluviated and eroded velocity profiles at 2 locations in the canyon reach for all runs. Left side shows relative depth z/h in linear scale, right side shows z/h in log scale. Profiles a), b) c) and d) were taken during the alluviated stage	32
Figure 18.	a) Bed and water surface topography during Run 5. Near bed vertical velocity during the b) initial stage and c) alluviated stage	38

Chapter 1.

Introduction

Bedrock canyons are river channels that are laterally confined on both sides by bedrock walls, which are often near vertical. Recent work has shown that bedrock canyons often develop deeply scoured pools that can be as deep as the channel is wide (cf. Venditti et al., 2014). Figure 1 shows the typical morphology of a bedrock canyon in the Fraser River system, with a series of deeply scoured pools within the laterally constrained canyon. The degree of lateral constriction can vary greatly in the Fraser Canyons. The proportion of lateral bedrock constriction relative to the upstream alluvial reach ranges from 20% to 75%. The constricted canyon reaches are characterized by partially exposed bedrock on the channel bed, while the unconstricted reaches both upstream and downstream of the canyon reach are alluviated with sediment. The scour pools often are associated with further local constriction of the channel within the bedrock canyon (Venditti et al., 2014, Hunt et al., 2018).

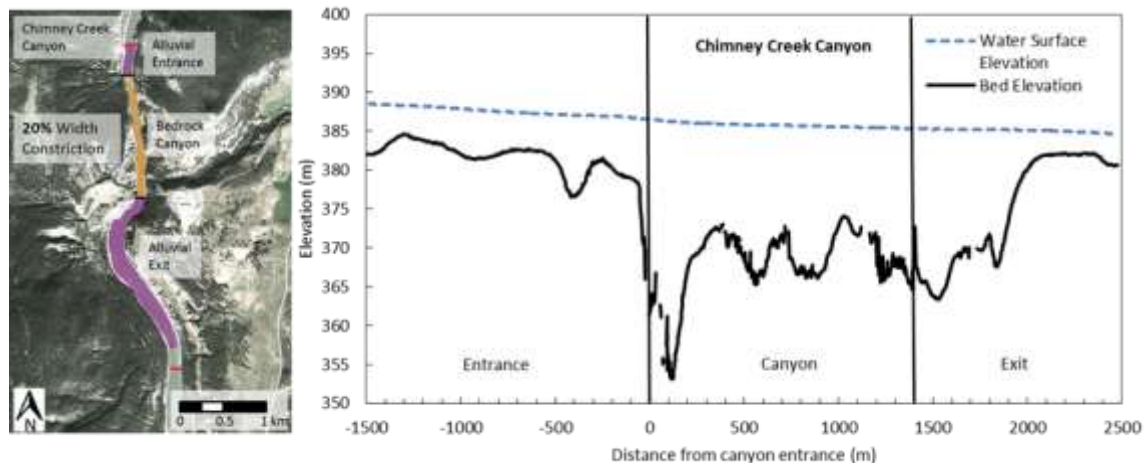


Figure 1. Geometry of Chimney Creek Canyon, Fraser River, showing long profile of the canyon with entrance and exit reaches. Water surface elevation at estimated discharge of 835 m³/s in September 2009.

The development of scour pools in bedrock rivers and its influence on the evolution of bedrock canyons has not previously been explored. The long-term evolution of channel geometry in bedrock rivers is set by large scale processes such as tectonic uplift rate and climate of the upstream drainage basin (Stark, 2006, Wobus et al., 2006,

Ferrier et al., 2013, Whipple and Dibiase, 2013). However, these large scale processes affect the entire reach of a bedrock river and cannot be used to explain local morphological features such as scour pools. Field observations show that scour pools are often found in laterally constricted bedrock canyons; such occurrences are unlikely coincidental. Therefore investigating local patterns of flow and sediment deposition associated with lateral constrictions might offer insight into why scour pools are formed in bedrock canyons.

Similar morphological features known as plunge pools have been observed in bedrock rivers, typically associated with plunging jets created by elevation drops at waterfall and dams (Manson and Arumugam, 1985, Ervin et al., 1997, Robinson et al., 2002, Pasternack et al., 2007, Scheingross and Lamb, 2017). Waterfalls and dam overfalls can be identified by the distinct drop in both the bed and water surface elevation upstream of the plunge pool. However, no obvious drop in water or bed elevation occurs upstream of scour pools in bedrock canyons. This leads to the question of whether these waterfall plunge pools and scour pools in canyons have genetically similar origins.

The processes driving vertical incision in bedrock rivers have been previously described as abrasion by saltating bedload or suspended sediment, and plucking of bedrock blocks in highly jointed rock (see reviews in Whipple et al., 2014; Lamb et al., 2015). Abrasion occurs when transported sediment impacts the bed with enough energy to detach small bits of the rock surface. The availability of tools for erosion and the efficiency of abrasion depend largely on sediment supply. At low sediment supply not enough tools are available for substantial erosion. At high sediment supply the bed is covered and shielded from impacts. The highest erosion rates occur at moderate sediment supply relative to the transport capacity of a river (Sklar and Dietrich, 2004). Sediments carried as suspended load can also contribute to the abrasion process as suspended sediments are exchanged with the boundary, impacting the channel bed to cause abrasion (Lamb et al., 2008). Abrasion has been shown to be the primary mechanism for bedrock incision in rivers flowing through massive crystalline rock (Karlstrom et al., 2008, Cook et al., 2013, Sanders et al., 2014, Beer et al., 2017).

Other rock erosion processes may be important depending on the structural features of the rock. Plucking is the removal of loose bedrock blocks from the channel

bed by lifting or sliding (Hancock et al., 1998) and depends on both the availability of loose pluckable blocks and sufficient power of the flow to transport the loose blocks (Chatanantavet and Parker, 2009). Plucking can be up to an order of magnitude more efficient (Whipple et al., 2000, Lamb and Fonstad, 2010, Baynes et al., 2015, Larson and Lamb, 2016), however plucking is an important process only where rivers are flowing over well-jointed bedrock (Lamb and Fonstad, 2010, Larson and Lamb, 2016) or rock that has developed a battered layer with loose blocks (Chatanantavet and Parker, 2009). Other processes such as cavitation and dissolution are capable of eroding bedrock locally, but have not been shown to contribute significantly to the erosion rate in bedrock rivers (Arndt, 1981, Hancock et al., 1998).

While the processes driving vertical incision in bedrock rivers have been described and in many circumstances modeled, the mechanisms for lateral erosion of rock banks and canyon walls that are important for setting channel morphology, are less well understood. Finnegan et al. (2007) argued that lateral erosion occurs when the bed alluviates and bedload moves along the margins of the channel. Fuller et al. (2016) suggested that lateral erosion occurs by sediment particles impacting an alluvial cover and being deflected toward the side walls, which causes abrasion to the base of the side walls over time. Other studies have shown that the erosion focus shifts from vertical to lateral erosion under high sediment supply, as alluviation of the channel bed promotes sediment impacts on the exposed channel walls (Turowski et al., 2008, Yanites and Tucker, 2010, Nelson and Seminara 2011, Beer et al., 2017).

Another mechanism for lateral erosion is associated with the non-uniform flow in bedrock canyons (Venditti et al., 2014). Where rivers enter a laterally constricted bedrock canyon, the flow accelerates and plunges towards the bottom of the channel, creating a high velocity core close to the channel bed. The high velocity core then diverges toward the sides and causes up-welling along the channel walls. Divergent flow along the bed could drive sediment to undercut the channel walls without an alluvial cover, which could widen the channel through the toppling of overhanging walls (Goodman and Bray, 1977, Weissel and Seidl, 1997, Lamb and Dietrich, 2009, Venditti et al., 2014).

The presence of non-uniform flow through constricted bedrock canyons presents a distinct problem for understanding the evolution of bedrock canyons through time. It is

not clear whether the non-uniform flow field is a result of the scour pool morphology or whether the non-uniform flow created by a lateral constriction causes the deeply scoured pool morphology. It would not be practical to observe the formation of a scour pool through field studies, due to both the difficulties in precisely tracking small changes on the channel bed in a bedrock canyon and the fact that significant incision in bedrock occurs over geological time scales. Therefore a flume experiment is better suited to study scour pool morphology, since the bedrock can be replaced with much faster eroding substitutes that behave similarly under sediment impacts, and the changes in the scour pool over time can be measured in controlled settings.

Here, we explore the formation of scour pools in bedrock canyons. The specific objectives are i) to investigate how lateral constriction of bedrock canyons can influence flow dynamics, rock erosion patterns and sediment deposition, ii) to identify the necessary conditions to initiate the formation of a scour pool in a bedrock canyons, iii) to observe how bedrock scour pools evolve over time in terms of vertical incision, lateral expansion, and migration, iv) to determine whether an equilibrium morphology exists for scour pools where a maximum depth and width are reached, and v) to explore the role of scour pool formation in the evolution of bedrock canyons.

Chapter 2.

Methods

2.1. Experimental setup

Experiments were conducted in a 490 cm long, 45 cm deep flume, with a width of 10.2 cm in the constricted canyon reach, and 20.4 cm in the unconstricted alluvial reaches, creating a 50% width constriction in the canyon. The constriction was formed using a Styrofoam back wall and inset Plexiglas front wall (Figure 2). A variable speed pump was used to recirculate water and sediment.

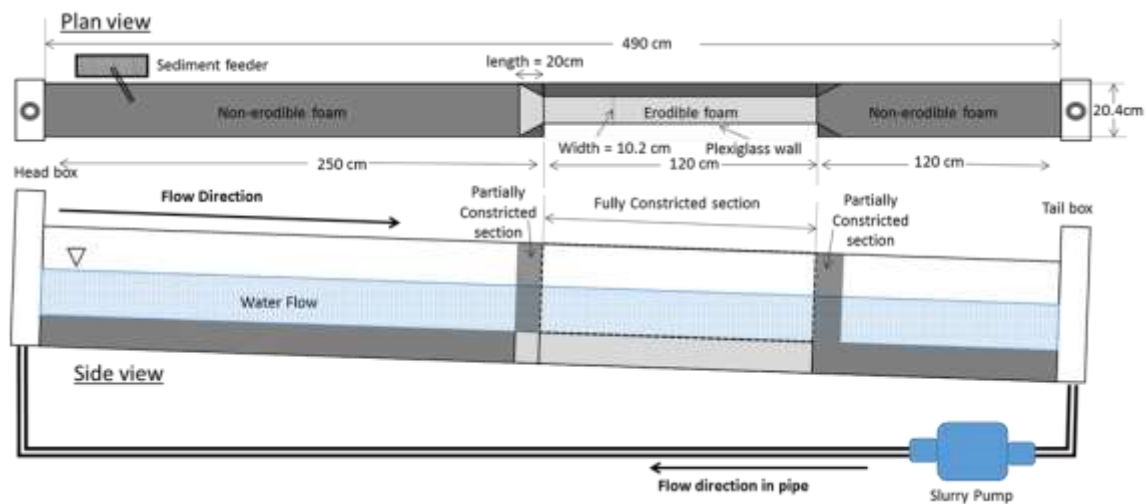


Figure 2. Schematic of the flume setup showing lateral constriction in the canyon reach of the channel (not to scale).

In total 5 runs were undertaken to compare the difference in erosion rate between two different sediment sizes. Runs 1, 3, and 4 used sediment with a D_{50} of 2.2 mm and a range of 1.6 to 3.2 mm, which is the smallest grain size that could effectively erode the bed material, before viscous damping starts to significantly diminish the impact energy (Scheingross et al., 2014). Runs 2 and 5 used coarser sediment that had a D_{50} of 4.8 mm with a range of 4 to 5.6 mm. This sediment was substantially larger than the finer sediment while still being able to pass through the pump. Both sediment materials were predominantly sub-angular in grain geometry. For each grain size a discharge was

chosen, for which transport through the constricted reach was possible without permanent alluviation, while allowing alluviation in the unconstricted reaches.

Two types of foam were used in the experiment. Non-erodible insulation foam was used to make the channel bed for the unconstricted reaches and the supporting pillars, so that no erosion would occur where we expected persistent sediment cover to form. The channel bed of the constricted reach was made from erodible closed-cell polyurethane foam (CCPF) which, according to the manufacturer, has a tensile strength of 0.32 MPa and density of 4lb/cft (64.06 kg/m³). This type of erodible foam is a reasonable substitute for bedrock, as tests have shown the same scaling relation between erosion rate and tensile strength applies to bedrock, concrete, and this type of foam (Scheingross et al., 2014). Furthermore, the foam does not deform plastically under impacts from the sediments used in this experiment (Lamb et al., 2015). The CCPF is also not erodible by water as evidenced by the fact that each run started with 10 hours of clear water flowing through the flume without any CCPF erosion.

The main CCPF (erodible foam) block used for the bed of the canyon reach was 122 cm long, 10.2 cm wide and 6 cm thick for Run 1, which had to be terminated before an equilibrium condition was reached because the foam nearly eroded all the way through. Runs 2 to 5 used a thicker 10 cm block to enable longer run times. The canyon entrance was defined where the canyon was fully constricted to 10.2 cm, which coincides with the main erodible foam block (Figure 2). Upstream of that, there was a section that transitioned from a width of 20.4 to 10.2 cm wide over a 20 cm distance, and there was another 20 cm section downstream of the canyon that transitioned from 10.2 to 20.4 cm. In order to ensure that erosion did not start at the junction between the non-erodible and erodible foam, a separate block of erodible foam was used for the bed at the canyon entrance through the width transition (Figure 2). For Run 1 this piece of erodible foam was 50 cm long, 20.4 cm wide and 10 cm thick. Observations from Run 1 showed that the bed was fully alluviated 10 cm upstream of the canyon entrance and no erosion occurred beyond that point, therefore subsequent runs used a 10 cm long non-erodible foam piece in the constriction.

2.2. Experimental procedures

Each run consisted of four stages: an initial stage, a sediment feeding stage, an alluviated stage, and an eroded stage. During the initial stage (Stage 1), water flowed with no sediment in the flume for 10 hours, during which the initial bed and water surface elevations were measured, together with the mean and near-bed velocity along the channel at 10 cm intervals, and 5 velocity profiles (see below for details of velocity measurements). The 10 hours of Stage 1 were not counted towards the total run time since no erosion occurred with only water in the flume.

In the feeding stage (Stage 2), sediment was added to the flume at a constant rate using a sediment feeder positioned at the upstream end of the flume, until the flume had enough sediment to provide transport through the canyon reach and no substantial change in the sediment deposits up and downstream of the constricted canyon reach. During this period, sediment was recirculated, so the feeder was effectively increasing sediment supply to the channel through time. The feed rate was set in consideration of the tools-and-cover effect; if too high, the canyon reach would alluviate and if too low, there were not enough tools to erode the bed. The feed rate was effectively optimized to maximize the erosion rate in the canyon reach. The sediment feed rate was 195 g/min for finer runs (1, 3, 4) and 260 g/min for coarser runs (2, 5). The feeding period was 4.5 hours. Then an additional 1.5 hours was given for sediment within the flume to stabilize, adding to a total of 6 hours to the run. These 6 hours were counted towards the reported run time for the each run, since foam material began to erode when sediments were added to the flume.

In the alluviated stage (Stage 3) of the experiment, the bed was covered by sediment upstream and downstream of the canyon with sediment passing through the canyon and eroding the CCPF block. The alluviated mean and near-bed velocity, along with velocity profiles where depth permitted, were measured at the beginning of this stage, right after the sediment deposition has stabilized but no significant erosion had occurred to the CCPF bed. Alluviated bed elevations, water surface elevations and pool depth were measured every 24 hours through Stage 3 of the runs. The runs were also paused every 24 hours for ~30 minutes to measure scour pool depth. During each pause, water was drained and sediment was cleared from the pool, which allowed for more accurate depth measurements without interference from the flow or sediment. The

flume was then refilled to the same water level and using the same temperature water before resuming. Sediment transport rate was measured periodically by placing a sieve over the tail box recirculation drain to catch all sediment exiting the flume. Each sample was collected over 5 minutes, and 5 samples were taken during each run to establish the flux rates during the alluviated stage.

The criterion for reaching the end of the run was that the scour pool had stopped vertically incising. This was considered achieved when two or more consecutive measurements showed little to no erosion within the pool over a 24 hour period. The eroded stage (Stage 4) was reached after the pool had stopped eroding. The flume was left running for a few additional hours in order to take the final set of velocity measurements, but this time was not included in the total run time. Only Runs 2, 4 and 5 were run to equilibrium morphology. Runs 1 and 3 were terminated early due to problems with the setup. The foam block used in Run 1 was not thick enough to complete the run. The bed slope for Run 3 was set too low, which resulted in reduced transport rates and lack of tools for erosion within a reasonable time frame. However, Runs 1 and 3 do provide some useful comparative data that are reported where available and relevant.

2.3. Observations

Channel bed elevations and water surface elevations were measured using rulers attached to the Plexiglas side wall, with reference to a leveled laser beam above the channel. The rulers covered a range from 200 cm upstream of the canyon entrance to 230 cm downstream of canyon entrance at 10 cm intervals (Figure 3). Within the canyon reach, pool formation depth was measured by lowering a narrow ruler down to the bottom of the pool, and then reading the ruler with reference to the initial non-eroded elevation. This was done every 24 hours, at 5 cm intervals for the first 60 cm of the canyon reach, and 10 cm interval for the last 60 cm.

Velocity measurements were taken using a downward looking Nortek Vectrino Acoustic Doppler Velocimeter (ADV) at 50 Hz. White acrylic paint was added as seeding materials to improve velocity measurement signal quality. ADVs rely on measuring the Doppler effect of fine suspended particles passing through the sampling volume. The mean flow velocity was measured at 0.6 of the flow depth below the water surface

(0.4d). The near-bed velocity was measured 0.6 cm above the channel bed, with a 0.4 cm high sampling volume in the vertical dimension. This depth was high enough so that sediment and channel bed would not interfere with the sample volume, but also low enough to be within the bottom 5-10% of the flow depth. Measurements were taken at 10 cm intervals along the channel, with each location corresponding to the position of the rulers used in elevation measurements. Measurement locations ranged from 150 cm upstream of the canyon entrance to 200 cm downstream of the canyon entrance, with the canyon reach ending at 120 cm downstream. Measurements were not taken further upstream and downstream due to unstable flow near the head box and tail box.

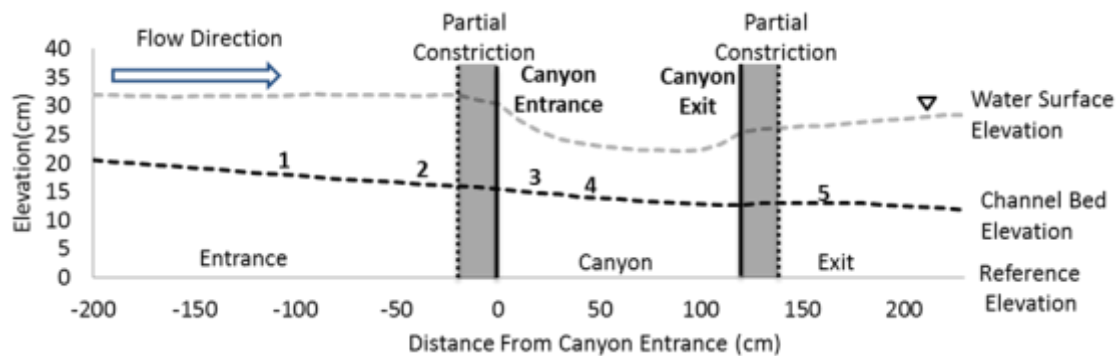


Figure 3. Initial water surface elevation, bed elevation and reference elevation for Run 1. Numbers 1-5 indicate the location of the 5 ADV velocity profiles.

Velocity profiles were also taken at 5 locations: two in the entrance reach, two inside the canyon reach, and one downstream of the canyon (Figure 3). The position of the sampling volume for the ADV was 4.6 cm below the probe transducers. The probe head needed to be submerged in water to get accurate measurements. As a result, the top 4.6 cm of water column could not be measured, which was the upper 30-40% of the flow depth.

Velocity data were processed using WinADV version 2.031 developed by the U.S. Bureau of Reclamation (Wahl, 2000). The ADV software provides signal quality information in the form of a correlation coefficient r_{ADV} and indicates that the signal may be dominated by noise when r_{ADV} does not exceed 0.7. However, it has been recognized that signal quality is reduced in highly turbulent regions of flow due to shear in the sampling volume and that reliable data may still be collected when r_{ADV} is <0.7 (Wahl, 2000, Martin et al., 2002). The mean r_{ADV} for velocity measurements taken in the entrance and canyon reaches was consistently $>90\%$. However, the average correlation

for measurements taken in the exit reach ranged from 60-70% where the flow was expanding and highly turbulent.

Photographs were taken during each stage using two Nikon D90 DSLR cameras. The first camera was mounted in a fixed position pointing at the canyon entrance from the side, capturing the first 60 cm of the canyon reach, taking photos at 10 minute intervals for the entire run time. A second camera used to capture the top-view was mounted right above the exit of the canyon reach pointing down and forward, which captured the entire canyon reach and entrance reach all the way up to the head box. The top-view camera was unable to see the channel bed when water was flowing due to turbulence, so these photos were taken during each 24 hour pause when the flume was drained. All photos taken during the experiments were corrected for lens distortion using Adobe Photoshop.

2.4. Data analysis

2.4.1. Calculating erosion volume and rate

Erosion rate was calculated by: 1) subtracting the dry CCPF block mass before and after the run, 2) measuring the volume eroded using photographs of CCPF block slices after the run, and 3) measuring the eroded volume during the run as the product of the depth of scour and its width. In the first method, eroded mass was converted into volume using the known density of the foam. This method accurately establishes the exact amount of foam eroded in each run, however it does not provide any information on where the erosion occurred or if the erosion rate changed during the run. The accuracy in estimating overall erosion rate is high for this method, but it offers no information on erosion pattern.

Method 2 required slicing the CCPF block into 1 cm thick slices to show the cross-section of the foam bed. Then photos were taken of each slice and imported to ArcGIS where the photos were converted to black and white, with the white area representing the remaining foam and black area representing the eroded foam. The area eroded from each slice was calculated as the total number of white pixels minus the total area of the slice, known from initial dimension of the CCPF block. The total volume of foam eroded could be calculated by multiplying the area eroded by the thickness of each

slice and summing for all the slices. The accuracy of this method is not as high as Method 1 because there is some uncertainty in the width of each slice and the measurements, but this method offers more information on erosion patterns. Method 2 produced a cumulative erosion volume that is slightly lower than Method 1 for all runs, which suggests some systematic deviations between the two methods.

Method 3 was used to track erosion rate within the pool, using the pool depth measurements every 5 cm in the downstream direction every 24 hours. The volume eroded was calculated by assuming a rectangular cross-section and multiplying the depth, width, and distance between each measurement. This method is not as accurate as Methods 1 or 2, however, this method is more useful in describing the erosion pattern and tracking the changes in erosion rate through time, whereas the Methods 1 and 2 could only be used at the end of the experiment.

2.4.2. Shear stress calculations

Shear stress was calculated using 3 methods. For the 5 locations where a velocity profile was available, a line was fitted between the natural logarithm of elevation above the bed ($\ln z$) and $u(z)$, where u is the velocity at z . The line was fitted through all available velocity measurements, from lowest point at 0.6 cm above the bed up the highest point at $z/h = 0.6$ to 0.7 depending on flow depth. The shear velocity was calculated using $u^* = \kappa a$, where κ is the Karman constant (0.41) and a is the slope of the line. The shear velocity was then used to calculate the shear stress from $\tau = \rho(u^*)^2$, where ρ is the density of water.

For all other locations where only the mean velocity and near-bed velocity were measured, the same method was used to calculate the shear stress using the gradient between the two points. The shear stress from the profile (τ_{pr}) and two-points (τ_{2p}) were checked against each other to ensure the two point gradient faithfully matched the estimates from the full profiles (see results). Shear stress was also calculated from the near-bed Reynolds stress, calculated as

$$\tau_{rs} = -\rho \overline{u'w'} \quad (1)$$

where

$$u' = u_i - \bar{u} \quad (2)$$

$$w' = w_i - \bar{w} \quad (3)$$

and u_i and w_i are instantaneous velocities in the downstream and vertical directions, \bar{u} and \bar{w} are mean velocities, and u' and w' are velocity fluctuations about the mean values at the measurement locations, obtained using ADV measurements at 50Hz frequency.

2.4.3. Entrainment threshold calculations

The threshold shear stress, mean velocity and near-bed velocity required to entrain sediment into bedload were calculated for comparison to the measured values. The threshold shear stress required for sediment entrainment in the flume was calculated using the Shields relation (1936):

$$\tau_c = \tau_c^* (\rho_s - \rho) g D \quad (4)$$

where τ_c^* is the dimensionless critical Shields number, ρ_s is the density of sediment, g is gravitational acceleration, and D is the grain size. For simplicity, we use $\tau_c^* = 0.045$ for the gravel sized sediments used in this experiment (Brownlie, 1981). The threshold mean velocity and near-bed velocity required for sediment entrainment were calculated using the law of the wall. The threshold mean velocity was calculated from

$$\bar{U}_c = \frac{u_c^*}{\kappa} \ln\left(\frac{h}{z_o}\right) \quad (5)$$

where u_c^* is the shear velocity calculated from τ_c , h is the reach average flow depth, and z_o is the plane of zero velocity above the bed, estimated using $z_o = 0.1D_{84}$ from Whiting and Dietrich (1991). Flow depth varied in the entrance, canyon and exit reaches, however the threshold mean velocity calculated is insensitive to variations in flow depth of that scale. The threshold near-bed velocity was calculated as

$$u(z)_c = \frac{u_c^*}{\kappa} \ln\left(\frac{z}{z_o}\right) \quad (6)$$

where z is taken as 6 mm, the height above the bed at which near-bed velocity was measured.

Chapter 3.

Erosion Pattern, Rate and Volume

3.1. Bed elevation and water surface elevation

Initially, the channel bed was clear of sediment with a pre-determined slope, and the water surface elevation was set so that the flow depth for the entrance and exit reaches were the same (Figure 3). The flow depth for the canyon reach was shallower due to higher velocity creating supercritical flow. Froude number in Run 1 was 0.38 for the entrance reach and 1.2 for the canyon reach (Table 1). Similar Froude numbers were found in other runs. There was no obvious hydraulic jump.

Figure 4 shows the changes in bed elevation that occurred as sediment was added to the flume and through each run. Sediment fed into the flume deposited upstream of the canyon entrance. This led to aggradation of the channel bed and increased channel slope, up to a point where the slope was steep enough to move sediment through the entrance reach and into the canyon reach. Sediments accelerated through the canyon reach due to the lateral constrictions, but then deposited in the exit reach where channel width expanded again. Aggradation occurred in the exit reach, increasing the local bed slope until sediments were able to pass through into the tail box and recirculate back into the entrance reach.

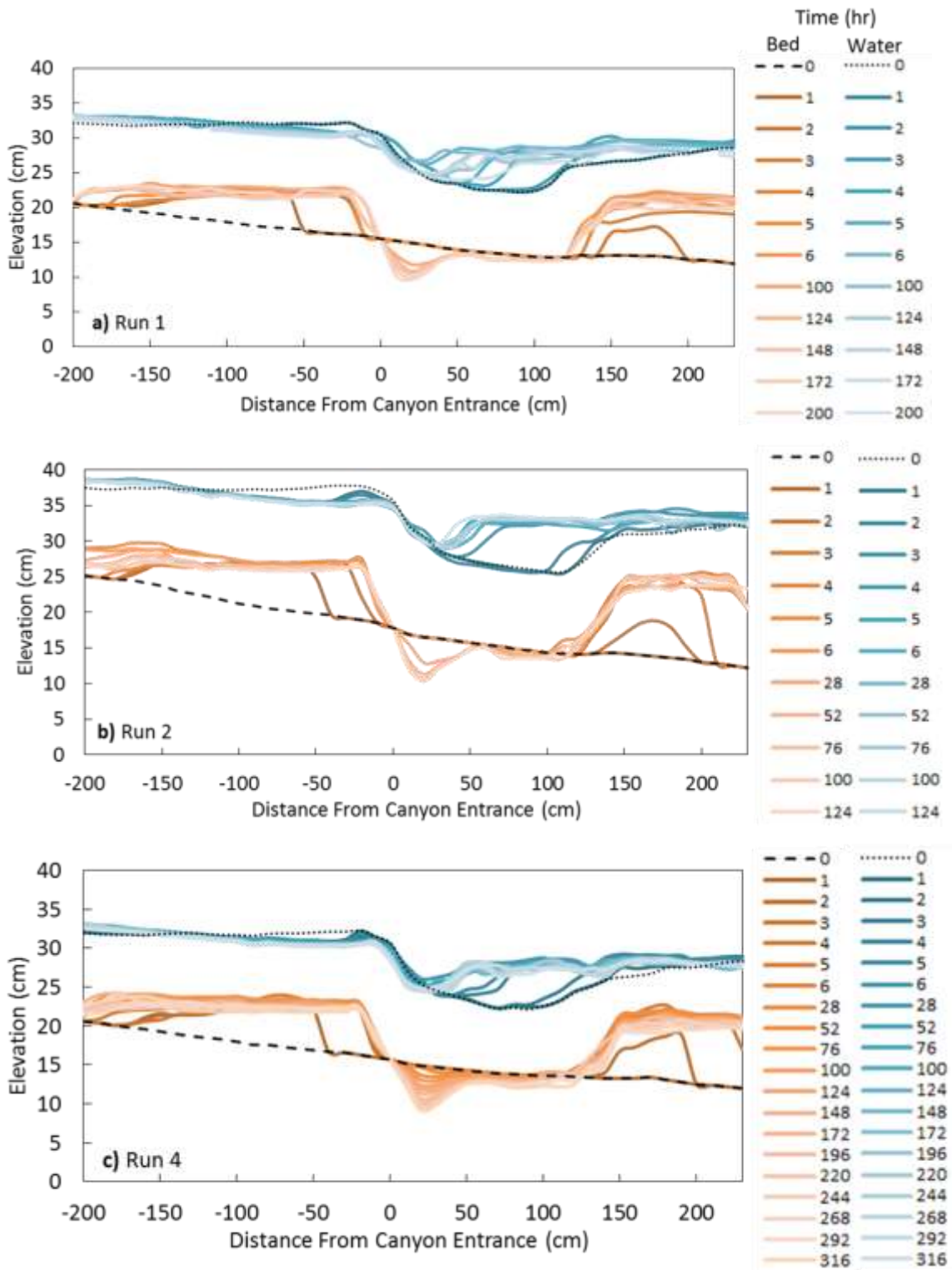
After sediment had been added to the flume, the entrance and exit reaches increased in bed elevation, due to alluviation of 4 to 6 cm of sediment that persisted throughout the entire run (Figure 4). Froude number adjusted so that it was 0.72 in the entrance and 0.75 in the canyon reach (Table 2). The canyon reach did not accumulate sediment cover and actually decreased in elevation due to vertical incision as the experiment progressed, although sediment traveling through the canyon reach did intermittently deposit at certain locations creating partial coverage. The flow depth of the entrance and exit reaches decreased as alluviation filled up much of the water column, but the overall water surface elevation increased only slightly (Figure 4). Flow depth increased in the canyon reach with alluviation.

Table 1. Summary of initial flume conditions for all runs.

Run ID	Discharge Q (m ³ /s)	Grain size Ds (mm)	Average flow depth (cm)	Flow depth entrance (cm)	Flow depth constriction (cm)	Flow depth canyon (cm)	Flow depth exit (cm)	Froude number entrance	Froude number canyon	Flume bed slope	Flume Water surface slope	Total run time (hr)
1	0.0117	2.2	13.1	14.4	15.0	10.0	14.4	0.38	1.19	0.0202	0.0084	200
2	0.0164	4.8	15.6	16.3	18.1	12.2	17.7	0.41	1.25	0.0300	0.0126	124
3	0.0117	2.2	13.0	14.7	15.1	10.1	14.1	0.34	1.19	0.0174	0.0084	124
4	0.0117	2.2	12.9	14.3	15.3	9.8	14.4	0.35	1.20	0.0200	0.0084	316
5	0.0164	4.8	15.3	16.7	17.9	12.0	17.7	0.39	1.24	0.0300	0.0121	124

Table 2. Summary of flume conditions at eroded stage for completed runs.

Run ID	Average flow depth (cm)	Flow depth entrance (cm)	Flow depth constriction (cm)	Flow depth canyon (cm)	Flow depth exit (cm)	Froude number entrance	Froude number canyon	Water surface slope	Transport rate qs (g/min)	Alluviation thickness entrance (cm)	Maximum eroded slot depth (cm)	Maximum eroded slot width (cm)
1	10.6	8.5	11.3	14.7	8.5	0.73	0.75	0.0114	261.1	4.8	5.1	2.2
2	12.8	9.9	15.2	18.8	10.3	0.82	0.71	0.0119	310.7	5.2	7	2.8
4	10.7	8.7	12.4	14.9	9.2	0.74	0.73	0.0109	271.4	4.5	5.7	2.5
5	12.1	9.5	15.4	17.6	9.5	0.83	0.75	0.0116	323.1	5.8	6.8	2.6



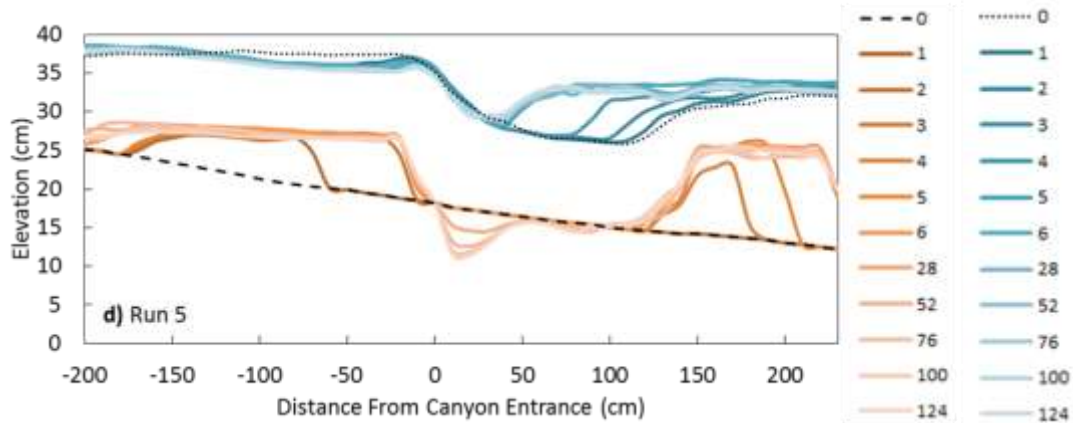


Figure 4. Change of bed elevation and water surface elevation over time for a) Run 1, b) Run 2, c) Run 4 and d) Run 5. Legend shows run time in hours for each measurement, dashed lines indicate initial elevations.

3.2. Erosion pattern

During the alluviated stage, sediment fully covered the entrance and exit reach, while partial sediment cover was observed in the canyon reach. A steady transport rate was established with the recirculation of sediment. Erosion on the channel bed occurred only within the canyon reach where the bed was partially exposed. Initially, a shallow groove was formed at roughly 10 cm downstream of the canyon entrance. The groove extended in both upstream and downstream directions from the initial position, while also rapidly incising downward into a narrow and deep slot (Figure 5). At the downstream end of the initial slot, a secondary pool developed with a center ridge and two sub-channels diverging to either side, each side channel then expanded in width, depth, and downstream distance, but eventually converged again near the end of the canyon reach. After around 24 hours into the run, the upstream extent of the pool migrated past the canyon entrance and into the partially constricted reach. The downstream extent of the pool was ~50 cm from the entrance. The width of the pool was set within the first 48 hours and remained fairly constant throughout rest of the experiment. The equilibrium dimension of the pool was reached when 2 consecutive depth measurements were within 1 mm of each other, which means less than 1 mm of erosion occurred over 24 hours and that the pool was unlikely to incise further. For runs with finer sediment, only Run 4 reached equilibrium after 316 hours (13 days). Runs 1 and 3 were stopped at 200 hours and 124 hours due to issues mentioned above. Both coarse sediment Runs 2 and 5 reached equilibrium after 124 hours (5 days).

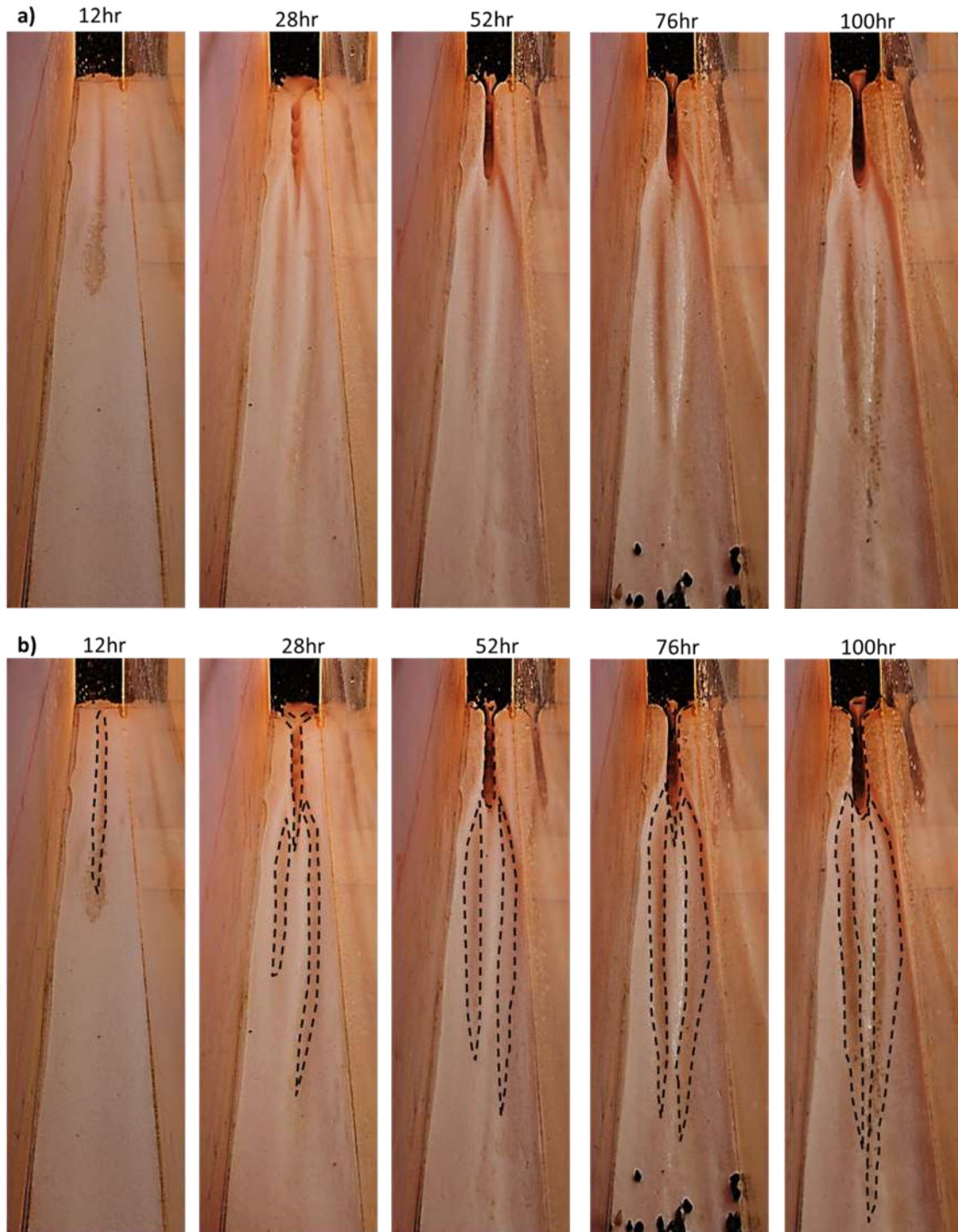


Figure 5. Erosion pattern from 12 hour to 100 hour for Run 5 showing the initiation and development of the primary pool and the secondary pool, within the constricted canyon. Panels a) and b) are the same images with and without the pool outlined using dashed lines.

The final pool was 50 to 60 cm in length, with a general V shape in the alongstream direction that had a steeper entrance limb and gentler exit limb (Figure 6). The maximum depth of the pool reached 5.5 cm for finer sediment and 7 cm for coarser. The width of the pool was 2 cm for finer sediment runs and 2.6 cm for coarser runs. The pool had a U-shaped cross-section with vertical and sometimes undercut sidewalls (Figure 7); the undercutting was most significant at 10 to 20 cm downstream from the canyon entrance where erosion rate was the highest.

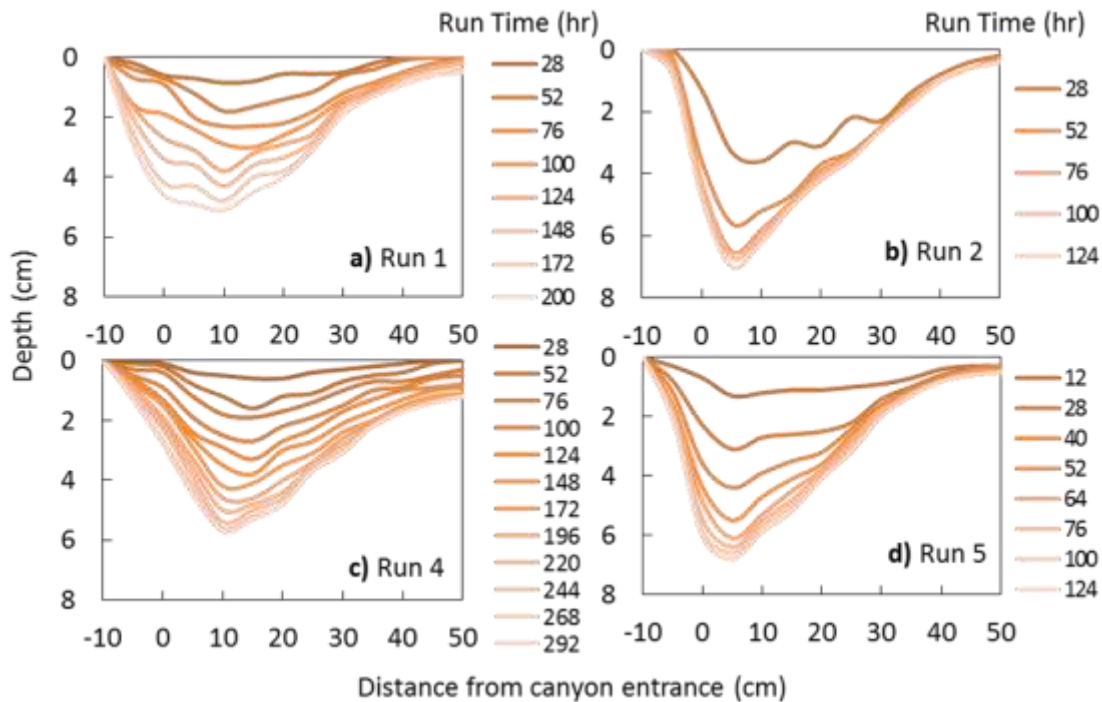


Figure 6. Depth of the pool formation over time for a) Run 1, b) Run 2, c) Run 4 and d) Run 5.

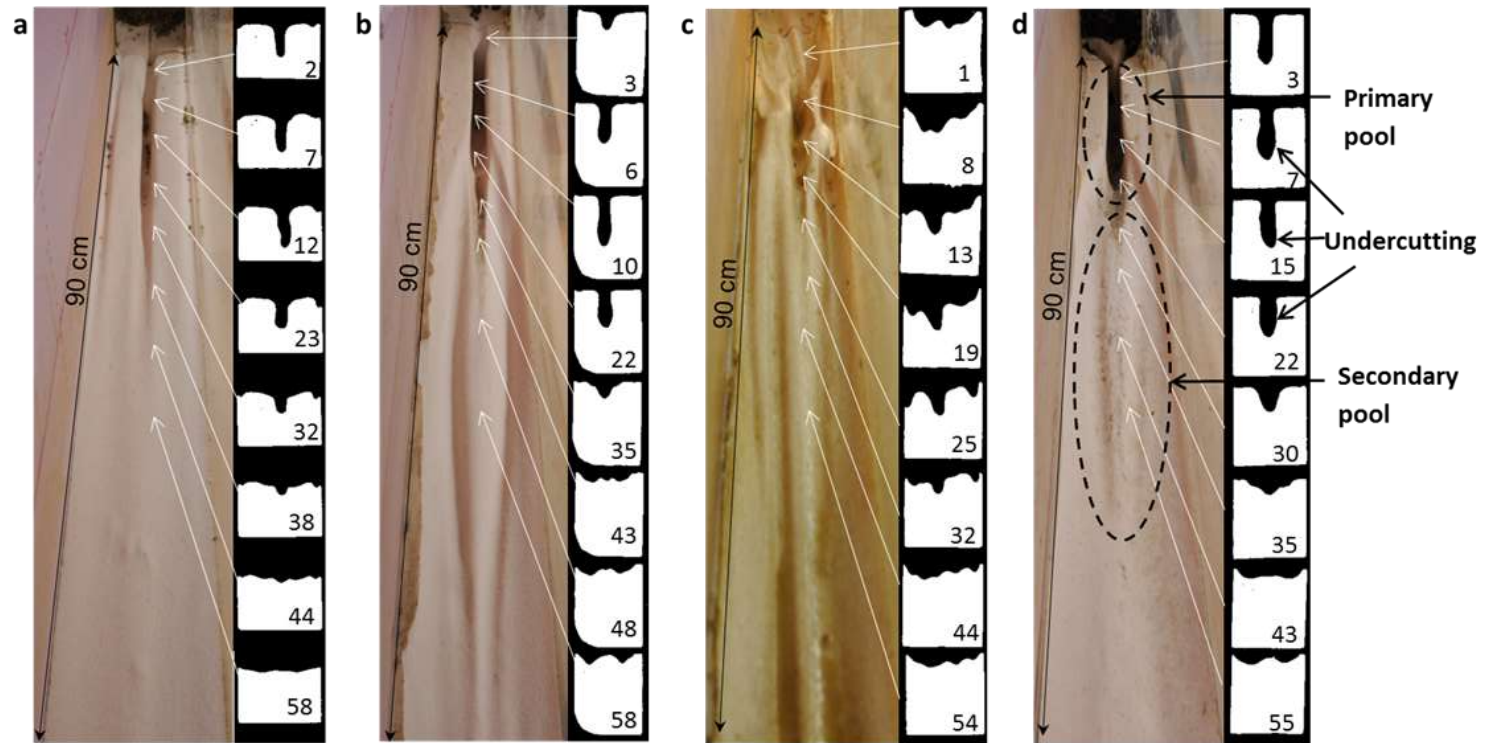


Figure 7. Foam slices showing cross section of the pool formation with reference to where each slice was taken from along the canyon reach for a) Run 1, b) Run 2, c) Run 4 and d) Run 5. Number is the bottom right of slices indicates distance from the canyon entrance.

3.3. Intermittent alluviation cycles

Sediment in the flume was observed to be moving in small bursts as opposed to a steady stream. As a result, the alluviation pattern in the canyon reach varied from almost no cover to sometimes complete coverage (Figure 8). The channel bed was constantly transitioning between covered and clear, in a cyclical pattern, and the frequency of each cycle varied depending on the size of each transport burst. The exact time of each cycle was difficult to determine from sequential photos taken at 10 minute intervals because multiple cycles could have occurred in-between each photo. However, visual observations indicated that the duration of each cycle was between 5 to 10 minutes and intermittent. Two consecutive photos showing similar alluviation coverage usually means a full cycle had occurred, and not that the alluviation remained unchanged during the time frame between photos. The alluviation cycle could influence the short-term incision rate due to the tools and cover effect, such that the clear stage of the cycle would not have enough 'tools' for erosion while high coverage would shield the foam from impacts, therefore most of the erosion occurred during the transitional stage between the two extremes.

3.4. Local erosion volumes and rates

Local erosion rates were calculated using Method 3, which was able to track the changes in erosion rate over time at each location within the pool. This method was used only to measure the first 50 cm of the canyon reach, and 10 cm upstream of the canyon entrance, which included only the first pool and not the rest of the canyon reach. Figure 9 shows the eroded volume and Figure 10 shows the erosion rate through time at various positions along the canyon.

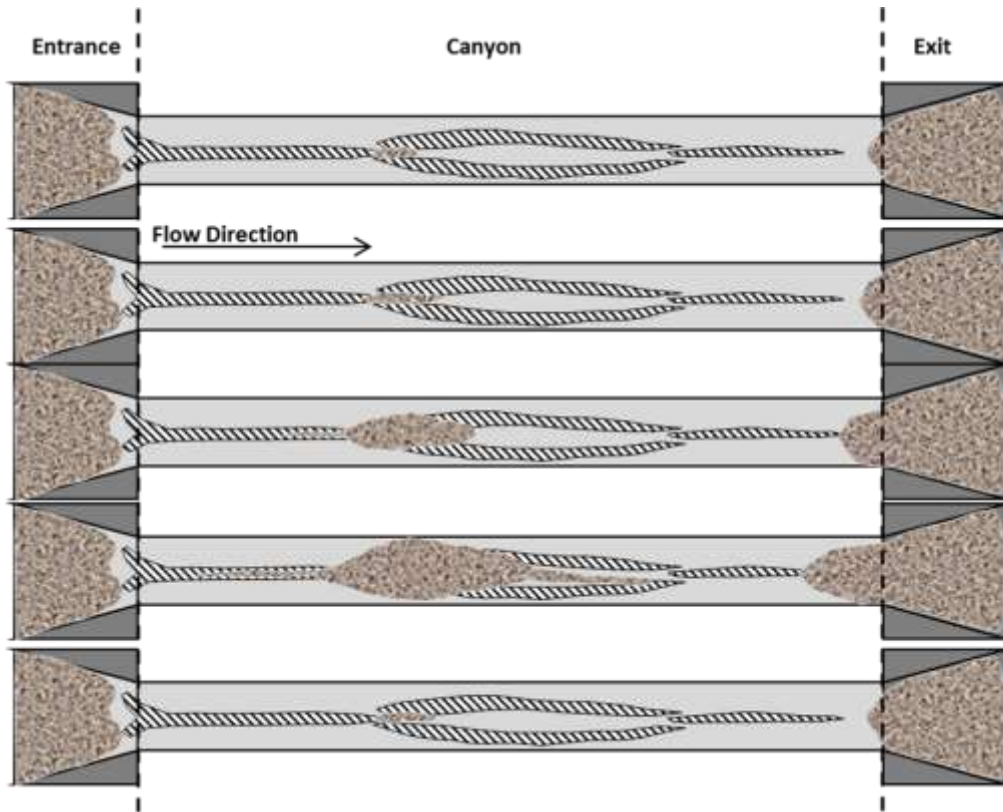


Figure 8. Illustration of a typical alluviation cycle that occurs during the experiment based on photos taken during the run, the channel bed constantly transitions between low sediment cover to high sediment cover, with varying degrees in each cycle.

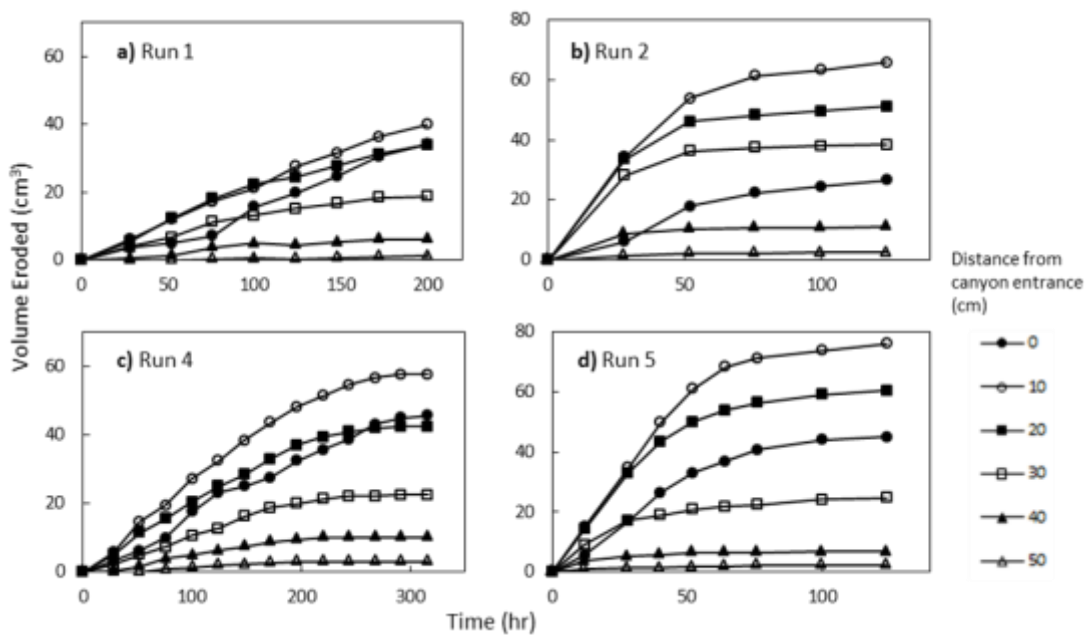


Figure 9. Volume of foam eroded over time at 6 locations within the pool formation a) Run 1, b) Run 2, c) Run 4 and d) Run 5.

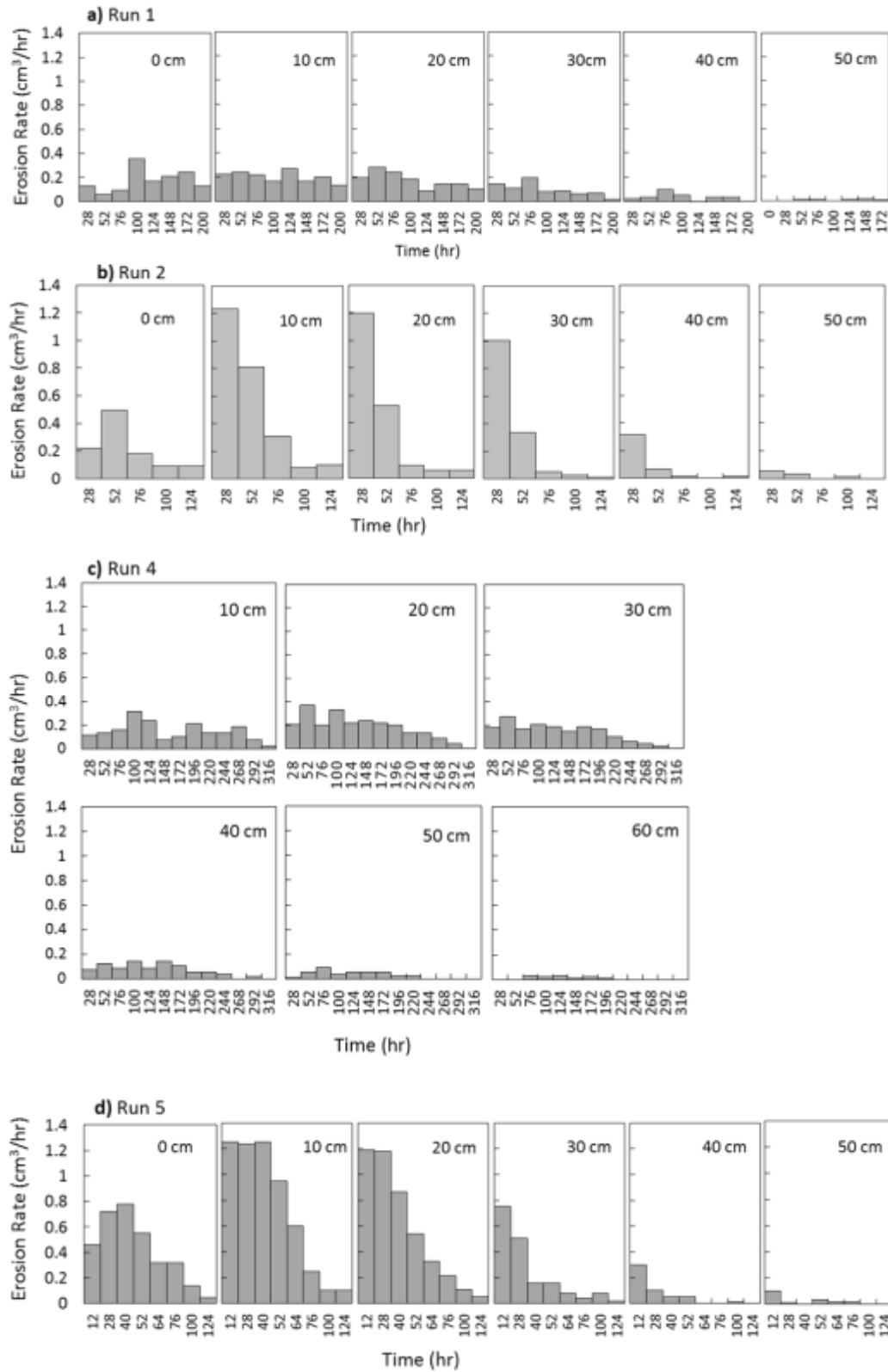


Figure 10. Local erosion rate over time at 6 locations within the pool for a) Run 1, b) Run 2, c) Run 4 and d) Run 5.

Erosion volume and rate varied spatially through the canyon. Erosion volume increased asymptotically until it reached steady state, except for Run 1 which was terminated early. The erosion rate was highest between 10 and 20 cm downstream of the canyon entrance and the deepest depth was at 10 cm (Figure 10). The erosion rate decreased moving upstream towards the canyon entrance and moving down downstream towards 40 to 50 cm (Figure 10). The lowest erosion rate was observed at 50 cm from the canyon entrance, where some erosion occurred within the first 24 hours, but then remained unchanged for the rest of the experiment due to persistent sediment cover, shielding the bed from further erosion at this location. The position where the highest or lowest erosion rate occurred was similar in all runs, but the actual volume eroded was higher in coarse sediment runs than fine sediment runs.

Erosion rate also changed with time at each location (Figure 10). Erosion rate was the highest at the beginning of each run, and gradually declined over time. However, at 0 cm the initial erosion was lower, because the pool had not yet migrated upstream towards the constriction. The variability of erosion rate over time was substantial. The highest erosion rate observed was $1.2 \text{ cm}^3/\text{hr}$ within the first 24 hours of the coarse sediment runs, but the erosion rate dropped to less than $0.1 \text{ cm}^3/\text{hr}$ near the end of the runs (Figure 10). Fine sediment runs follow the same pattern as coarse runs but at a lower magnitude and over longer time period.

3.5. Cumulative erosion volume and rates

The pattern in cumulative erosion volume coincides with the formation of the first and secondary pools (Figure 11). Erosion rate within the canyon reach showed a peak at 10 to 20 cm that corresponded to the location of the deepest part of the primary pool. A second, smaller peak is also visible at 60 to 80 cm that corresponded to the secondary scour pool. The lowest erosion rates within the canyon occurred at the exit of the first scour pool where a sediment patch persisted, and also near the canyon exit where flow velocity decreased as the channel became unconstricted.

Cumulative erosion rate was much higher in runs with coarser sediment than in runs of finer sediment. The erosion rate calculated for the two coarse runs differed by <3% ($10.68 \text{ cm}^3/\text{hr}$ for Run 2 and $10.38 \text{ cm}^3/\text{hr}$ in Run 5; Table 3). The erosion rate for finer runs deviated by ~33% ($4.25 \text{ cm}^3/\text{hr}$ for Run 1 and $5.68 \text{ cm}^3/\text{hr}$ for Run 4; Table 3),

but Run 1 was terminated early, so some difference is reasonably expected. The time required to reach equilibrium was only 124 hours for coarser runs and 316 hours in a finer run, meaning that coarser sediments are much more efficient at eroding the bed material than finer sediments.

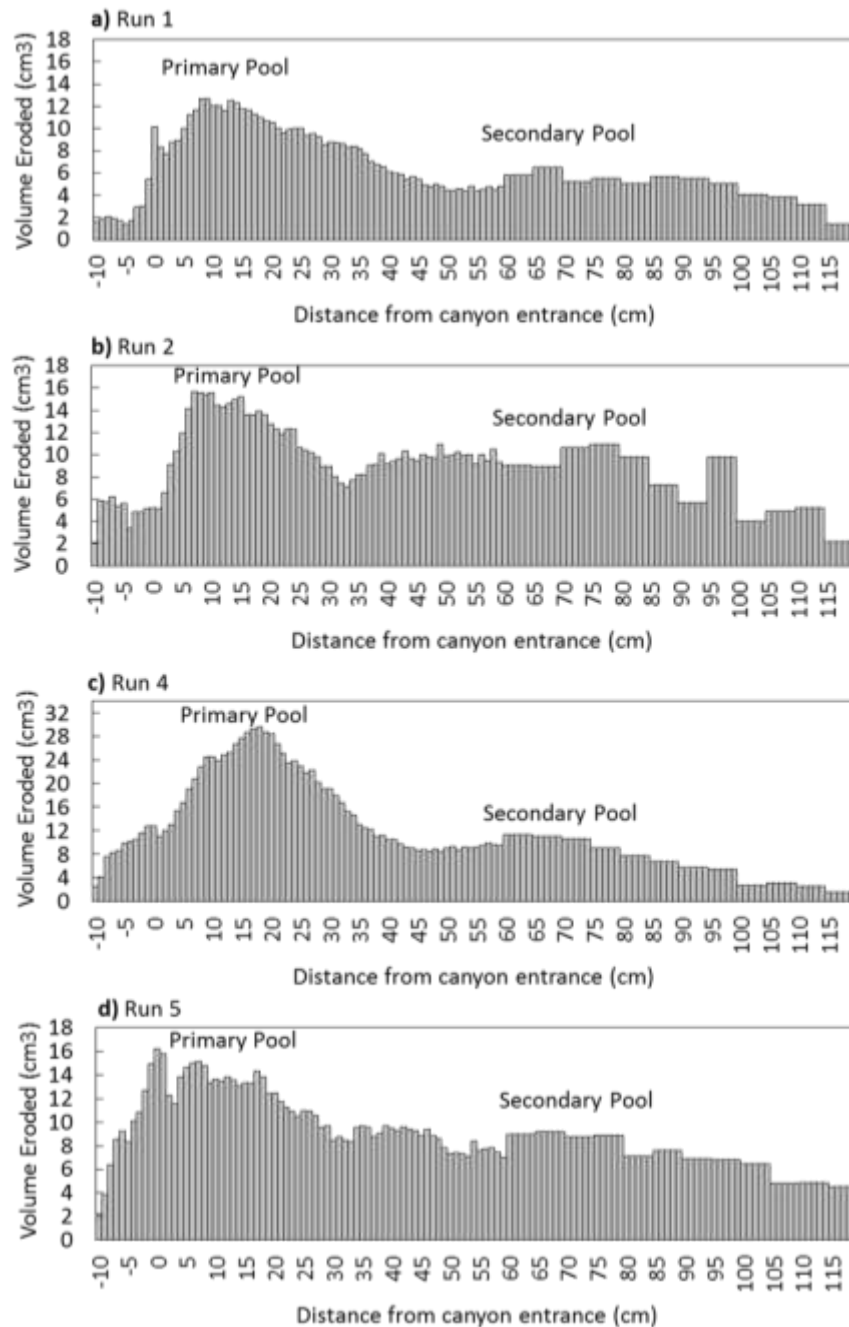


Figure 11. Final volume of foam material eroded at each location within the canyon reach, including 10 cm upstream of the canyon entrance shown as negative values, for a) Run 1, b) Run 2, c) Run 4 and d) Run 5.

Table 3. Cumulative erosion for the entire canyon reach, derived from 2 methods.

Run ID	Weight eroded (g) Method 1	Volume eroded (cm ³) Method 1	Weight eroded (g) Method 2	Volume eroded (cm ³) Method 2	Total run rime (hr)	Erosion rate (cm ³ /hr)
1	54.44	849.64	51.59	805.21	200*	4.25
2	84.88	1324.72	72.84	1136.86	124	10.68
4	115.06	1795.74	94.25	1470.98	316	5.68
5	82.44	1286.64	73.96	1154.24	124	10.38

* run 1 terminated at 200 hours, see Method section.

Chapter 4.

Patterns of Velocity and Shear Stress

4.1. Comparison of the shear stress estimation methods

The velocity profiles were not taken at enough locations to explore the patterns in shear stress through the canyon, but the two-point velocity gradients provide an opportunity to examine the alongstream distribution of boundary shear stress. Regressions are corrected to reduced major axis functional relations using Mark and Church (1977). Comparison between τ_{2p} and τ_{pr} reveals a nearly 1:1 relation (Figure 12a). Linear regression forced through the origin reveals the relation between the two methods has a slope of 0.99 and R2 value of 0.91. This shows that the two point profiles are a faithful representation of the shear stress. The relation between τ_{pr} and τ_{rs} also appears to be linear, but is not 1:1 (figure 12b) τ_{rs} is systematically lower than τ_{pr} by ~45% and the R2 value is much lower. Such discrepancies are not uncommon (Venditti, 2003, Yager et al., in review).

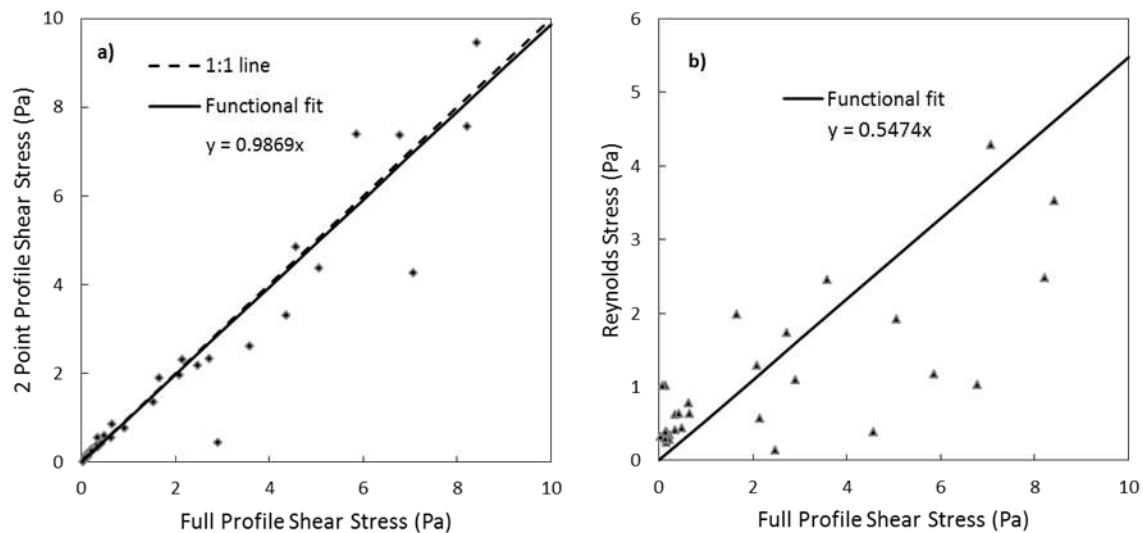


Figure 12. Comparison of shear stress calculated using the full profile method with a) the 2 point profile method and b) Reynolds stress method. Regressions are corrected to reduced major axis functional relations using Mark and Church (1977).

4.2. Velocity and shear stress distribution prior to sediment feed

Figure 13 shows velocity profiles into, through and exiting the canyon prior to sediment feed. Entering the canyon, velocity profiles are roughly log-linear (Figure 13a-d). Within the canyon, the profile taken 20 cm from the entrance is also log-linear but the flow accelerates substantially (Figure 13e-f). The profile taken at 50 cm from the canyon entrance reflects the accelerated flow (Figure 13e-f). Profiles are curved, with the highest velocity occurring at 0.2 to 0.4 of the flow depth and a decrease in velocity higher up the in water column (Figure 13g-h). Profiles downstream of the canyon show decelerating flow, but they do not fully adjust back to a log-linear profile (Figure 13i-j). Profiles instead exhibit a continuous linear increase in velocity with distance above the bed. Velocity profiles in the canyon and exit reaches suggest highly non-uniform flow.

Alongstream patterns of mean (Figure 14) and near bed velocity (Figure 15) confirm the patterns observed in the velocity profiles. The mean velocity was consistently higher through the canyon compared to upstream and downstream reaches (Figure 14a). Mean velocity was nearly constant between 40 to 60 cm/s in the entrance reach. Both mean and near-bed velocities began to increase ~10 cm upstream of the full channel constriction, where the channel is narrowing. Mean velocity increased until ~40 cm into the canyon, at which point velocities were nearly constant, although increasing slightly. The highest mean velocities were observed in the canyon reach with 120 to 140 cm/s. Mean velocity began to decrease within the canyon at 100 cm and decreased well beyond the canyon exit and the end of the constriction until 150 cm from the entrance (30 cm from the exit; 10 cm from the constriction end). Near-bed velocities mirror the pattern in mean velocity (Figure 15a).

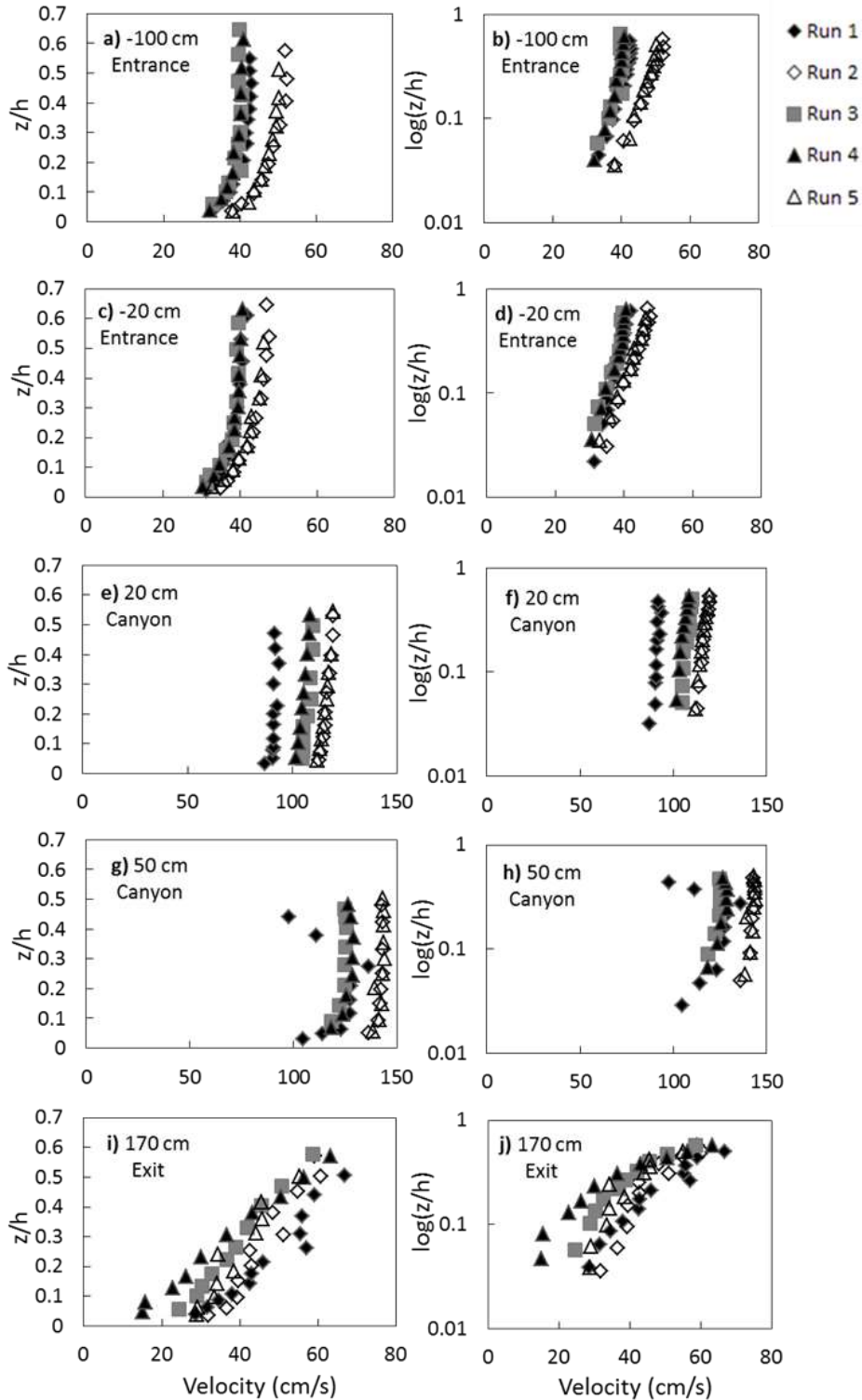


Figure 13. Initial velocity profile at 5 locations (Figure 3) for all runs, before sediment was added to the flume, left column uses linear scale for relative depth on y-axis, right column uses logarithmic scale for relative depth on y-axis.

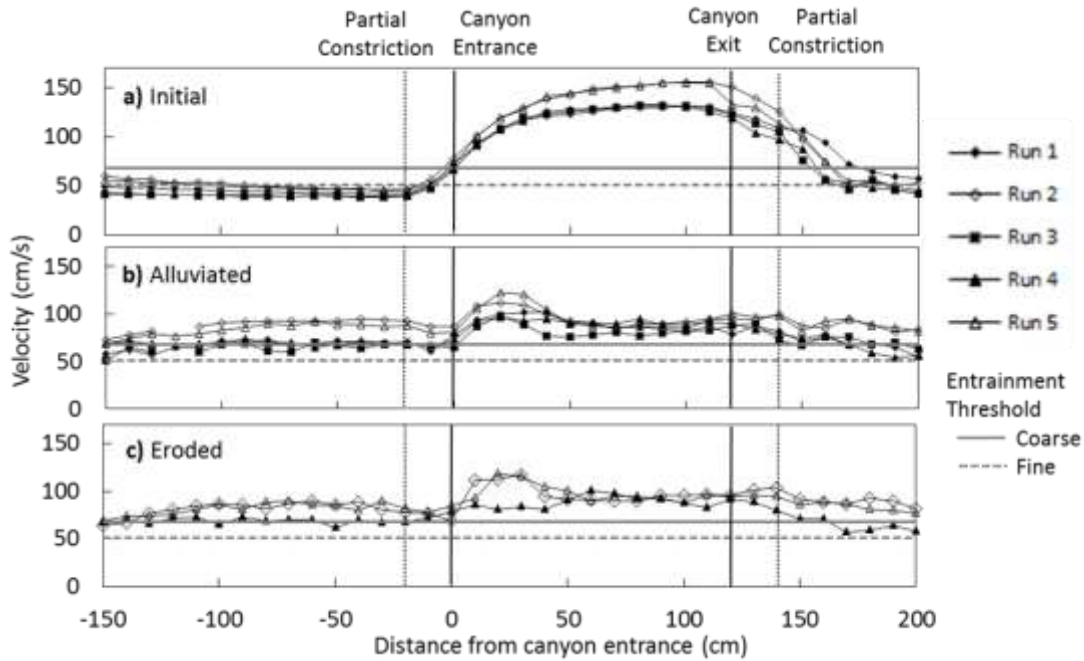


Figure 14. Mean velocity along the channel measured at $z/d = 0.4$ during the a) initial stage, b) alluviated stage and c) eroded stage.

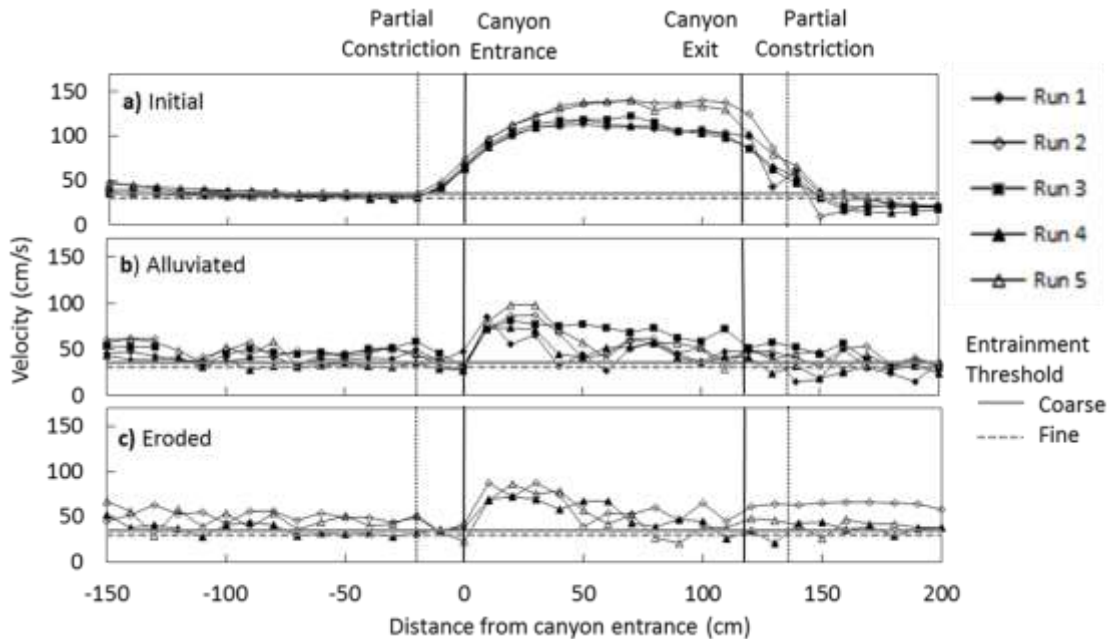


Figure 15. Near-bed velocity measured at 6mm above the bed during the a) initial stage, b) alluviated stage and c) eroded stage.

The alongstream variation in shear stress during the initial stage is different than during the alluviated and eroded stages (Figure 16). During the initial stage, τ_{2p} was between 0.3 and 0.5 Pa upstream of the canyon. Shear stress began to rise at the

canyon entrance to 1 Pa and increased further from 50 cm onward, up to 3 Pa at the canyon exit. A major spike up to 20 Pa occurred within the exit reach where flow was strongly decelerating due to the backwater. The alongstream pattern of near-bed Reynolds stress displayed similar patterns to τ_{2p} . Reynolds stress was 0.3 to 0.6 in both the entrance and the upstream half of the canyon reach, and then gradually increased to 1.2 to 1.5 Pa further down the canyon. A major spike up to 10 Pa occurred near the canyon exit where the flow was decelerating (Figure 16).

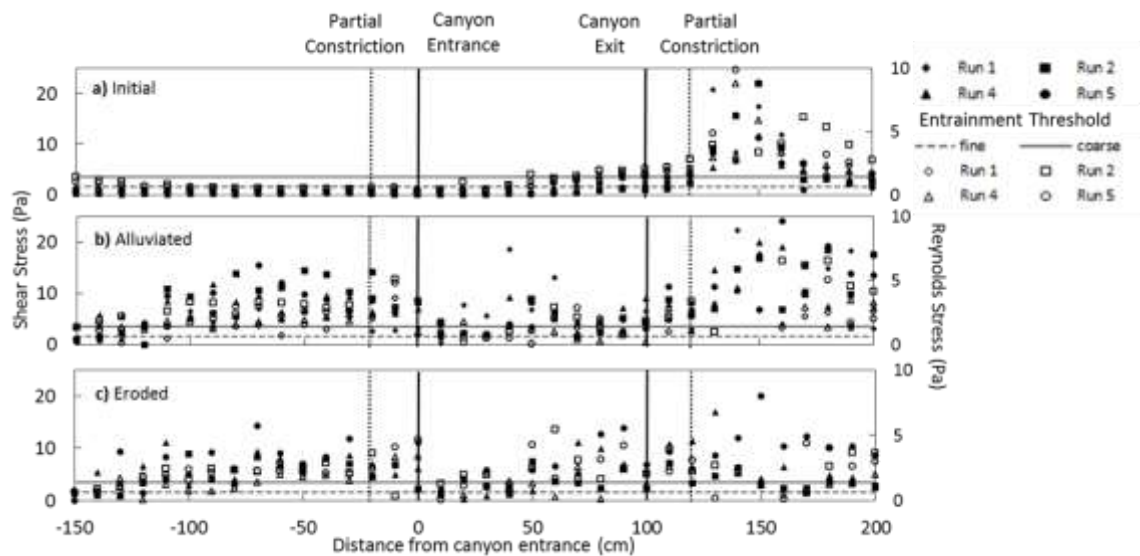


Figure 16. Shear stress derived from the 2 point profiles (solid points) and near-bed Reynolds stress (hollow points) along the channel measured during the a) initial stage, b) alluviated stage and c) eroded stage.

4.3. Velocity and shear stress distribution after alluviation and erosion

Alluviation of the bed, following the sediment feed but before the erosion, changed the distribution of both mean and near bed velocity. Both entrance and exit reaches had become fully alluviated with 4 to 6 cm of sediment cover, while the channel bed in the canyon remained partially and intermittently clear. Flow depth was too shallow in the entrance and exit reaches to obtain velocity profiles. Velocity profiles in the canyon displayed an S shaped curve (Figure 17). The lower portion of the water column had low velocities. There was a gradual increase in velocity up through the water column, reaching the maximum velocity at around 50% of flow depth.

The alongstream patterns of mean and near-bed velocity during the alluviated stage were different from the initial stage. Mean velocity entering the canyon was 70 to 90 cm/s. (Figure 14b). Mean velocity increased entering the canyon and peaked at the first 50 cm of the canyon reach up 120 cm/s. Further down the canyon reach mean velocity gradually declined to 90 cm/s, and continued to decline exiting the canyon down to 70 cm/s in the exit reach. Near-bed velocity displayed the same pattern as mean velocity but at a lower magnitude. During the eroded stage the alongstream distribution of velocity was similar to the alluviated stage (Figure 14c). The mean velocity was still 70 to 90 cm/s in the entrance reach and increased entering the canyon up to 120 cm/s within the first 50 cm of the canyon reach. Velocity decreased to 90 cm/s in the downstream half of the canyon reach and further decreased to 70cm/s in the exit reach.

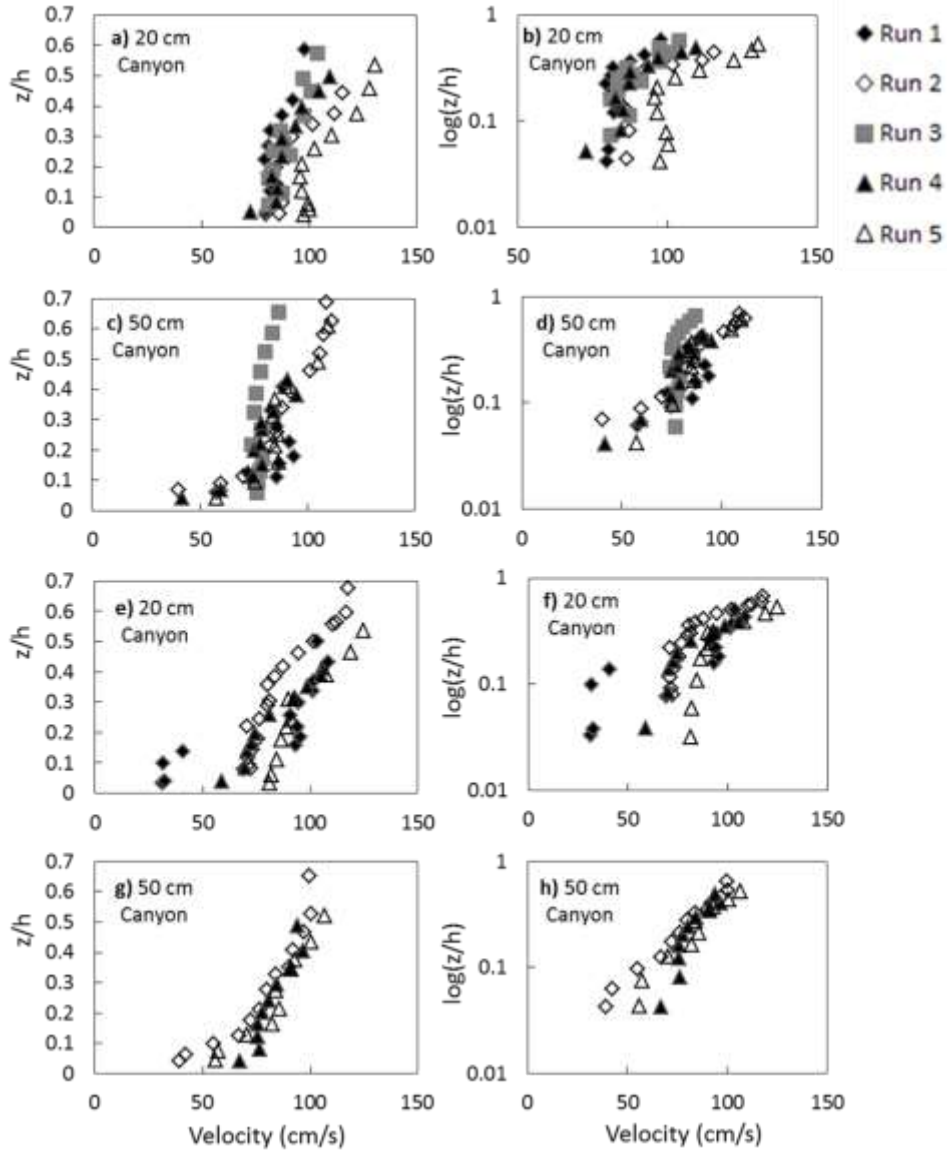


Figure 17. Alluviated and eroded velocity profiles at 2 locations in the canyon reach for all runs. Left side shows relative depth z/h in linear scale, right side shows z/h in log scale. Profiles a), b) c) and d) were taken during the alluviated stage

Shear stress during the alluviated stage was 5 to 15 Pa in the reach upstream of the canyon and increased approaching the constriction (Figure 16). Counterintuitively, shear stress decreased to 2 to 4 Pa at the canyon entrance but recovered to 8 to 10 Pa further into the canyon. This is exactly opposite of the alluviation pattern. A spike in shear stress up to 20 Pa occurred in the canyon exit. The alluviated stage and eroded stage displayed similar patterns of shear stress distribution. But the magnitude appeared to be lower in the eroded stage, with a more pronounced drop in shear stress at the

canyon entrance. Near-bed Reynolds stress was 2 to 4 Pa in the entrance reach, with higher values closer to the canyon reach. As with τ_{2p} , Reynolds stress counterintuitively dropped to 0.5 Pa at the canyon reach entrance, but recovered to 2 Pa again further down the canyon reach.

4.4. Velocity and shear stress relative to thresholds

The mean and near-bed velocities in both the entrance and exit reaches were below the sediment entrainment threshold during the initial stage, which is consistent with the observation that sediments fed into the flume initially deposited in the entrance and exit reaches and were only able to pass through those reaches by building up the bed, causing a spatial flow acceleration. Mean velocities upstream, within and downstream of the canyon exceeded the threshold for entrainment during the alluviated stage. Near-bed velocities through all three reaches were at or exceeded the entrainment threshold. In the entrance to the canyon, (0 to 50 cm) where the bed was generally clean of sediment the entrainment threshold was greatly exceeded. Where intermittent cover formed in the canyon, near-bed velocities were at or exceeded the entrainment threshold, which matches the locations of sediment deposition observed within the canyon reach, one being at the end of the first scour pool, and the other near the canyon exit.

Shear stresses in both the entrance and canyon reaches were below the critical shear stress for sediment entrainment during the initial stage, except when approaching the canyon exit, where the threshold is greatly exceeded, even though this is an area that experienced deposition. During the alluviated and eroded stages, the entrainment threshold was greatly exceeded upstream and downstream of the canyon. Within the canyon, shear stresses were generally below the entrainment threshold, particularly near the canyon entrance. This is entirely counter to expectations based on the alluviation patterns, suggesting that these parameterizations of shear stress are not well correlated with sediment particle motions.

Chapter 5.

Discussion

5.1. Observed and expected erosion pattern

Scour pools found in the Fraser Canyons often have an alongstream V-shape profile with slightly steeper slope at the pool entrance than at the pool exit. The first pool is usually found close to the canyon entrance (Figure 1). Most scour pools are also full channel width and confined by vertical sidewalls (Venditti et al., 2014). However, scour pools across different canyons or even within the same canyon varied in terms of depth, length and frequency, so it makes sense to compare the experimental results to the general morphology found in bedrock canyons rather than the dimensions of any one particular scour pool observed in the Fraser system.

The initiation and evolution of the experimental pool matches the expected patterns in terms of location, shape, and extent. Formation of the experimental pool initiated roughly 10 cm downstream of the canyon entrance and expanded in both length and depth over time, with a rapid initial incision followed by slower incision as the pool expanded both downstream and laterally. The primary scour pool had a V-shaped profile with a slightly steeper entrance limb and gentler exit limb (Figure 6). One major difference between the experimental scour pools and those observed in the Fraser River is that only a narrow slot of roughly 2 to 3 cm width formed down the center of the experimental channel. Sediment entered the experimental canyon reach down the center of the channel and concentrated in the center. This led to sediment impacts that carved a slot along the center line, which forced sediment to proceed along the same slot, incising it further. This positive feedback resulted in sediment transport being confined within the pre-existing slot and incising the slot deeper, trapping more sediment and preventing sediment from wandering into the sides of the channel. The slot itself did widen in the beginning, but reached maximum width quickly and remained largely the same width for the rest of the experiment.

However, undercutting in the slot was observed, indicating some degree of lateral erosion (Figure 7). Finnegan et al. (2007) suggested that lateral erosion in

bedrock rivers occurs when an alluvial cover forms, which deflects bedload away from the channel centerline and towards the walls. Fuller et al. (2016) showed that this occurs mainly due to sediment particles hitting the alluvial deposit and being deflected into the side walls. Other studies have also shown vertical incision shifts to lateral erosion when the bed becomes fully alluviated under high sediment supply (Turowski et al. 2008, Nelson and Seminara 2011, Beer et al., 2017), which could lead to undercutting of the side walls within the pool once the maximum depth is reached and sediment starts to deposit on the bottom of the pool.

Undercutting is an important mechanism for lateral expansion in bedrock canyons (Finnegan et al., 2007, Fuller et al., 2016). Bedrock surfaces are known to topple when on a steep slope, and undercutting increases the likelihood of overhanging walls collapsing into the channel under their own weight (Goodman and Bray, 1977, Weissel and Seidl, 1997, Lamb and Dietrich, 2009). The process would be further accelerated by existing fractures in the bedrock which could lead to toppling failures. Undercutting and toppling did not occur in the experiment because the walls are unlikely to collapse under the weight of the erodible foam and without any ability to fracture.

The formation of the secondary pool is due to sediment deposition at the downstream end of the first pool in the experiments. The deceleration of flow near the first pool exit results in a patch of sediment cover in the center of the channel. Persistent alluvial cover on the bed shifts erosion from channel center to the sides and even along the side walls (Finnegan et al., 2007, Nelson and Seminara, 2011, Fuller et al., 2016; Beer et al., 2017). The sediment patch not only shields the foam bed from particle impacts, but also deflects further incoming particles towards either side of the patch, creating two streams of sediment carving two slots along the sides separated by a ridge in the middle. The widest section of the secondary pool was in contact with the Plexiglass walls, which suggests that channel widening could occur if the walls were also erodible.

5.2. Influence of sediment on equilibrium morphology

Sediment is an important control on bedrock erosion; the rate of erosion is influenced by sediment size, sediment supply and pattern of sediment coverage (Sklar and Dietrich, 2001). Both the saltation abrasion (Sklar and Dietrich, 2004) and total load

erosion (Lamb et al., 2008) models predict that larger sediment has more energy per impact to abrade the bedrock. Furthermore, supply limited conditions result in higher erosion rates, provided there are enough tools to erode the rock (Sklar and Dietrich, 2004). The abrasion, plucking-macroabrasion model (Chatanantavet and Parker, 2009) also suggests the importance of sediment impact in fracturing the bed surface and preparing the bedrock for plucking; however, the plucking process could not be observed in our experiments due to nature of the foam material.

Our results support the idea that erosion rate is largely dependent on sediment size. Runs with coarser sediment (4.8 mm) reached equilibrium at over twice the rate of runs with finer sediment (2.2 mm). The equilibrium dimensions of the pool for coarser sediment runs were also deeper and wider. Larger sediments deliver more energy and remove more material from the bed with each impact.

Equilibrium dimensions of the pool were reached when further erosion within the pool ceased. The main reason for this was near constant alluviation of the pool bed. While initially the formation of a slot might increase erosion rate by forcing sediment to follow the same path within the slot, as the depth increases, the transport capacity within the slot decreases due to increased drag exerted by the sides of the slot. Eventually the slot reaches a depth where sediment starts to deposit and shield the bed from further erosion.

The equilibrium dimensions found here are for a constant discharge and sediment supply. In exploratory runs, it was observed that sediment cover could easily be cleared from pools by increasing water discharge. As such, changing factors such as the discharge, transport capacity, or sediment supply would alter the equilibrium morphology. In natural rivers where the discharge and sediment supply can vary by an order of magnitude, the equilibrium morphology of scour pools might be determined by the long-term climate and sediment supply from the drainage basin. However, results from the flume experiment confirm that the evolution of the scour pool does eventually lead to a negative feedback loop, where further incision is hindered by the existing morphology.

5.3. Plunging flow and vertical velocity

The occurrence of the scour pool slot in the experiments is coincident with downward directed velocities that occur after the bed has developed alluvial deposits. Near-bed vertical velocity measurements show a downward velocity vector near the canyon entrance with a magnitude of up to 10 cm/s, followed by an upward velocity vector of 5 cm/s at the canyon exit (Figure 18). The downward flow occurs at the canyon entrance and recovers back to a zero mean at 40 to 50 cm downstream of the canyon entrance, matching the extent of the scour pool. The downward velocity vector might be similar in nature to the plunging jets observed at waterfalls and dams, where the elevation drop caused by a negative step can create a high velocity jet that plunges towards the channel bed (Manson and Arumugam, 1985, Ervin et al., 1997, Robinson et al., 2002, Pasternack et al., 2007). Plunging jets are capable of carving plunge pools in bedrock rivers (Bollaert and Schleiss, 2003, Bennett and Alonso, 2005, Scheingross and Lamb, 2017). Plunging flows along with scour pools were observed in the Fraser Canyon, where high velocity flow plunged into a scour pool at the canyon entrance (Venditti et al., 2014). The results appear to suggest that scour pools may begin at a constriction due to the same mechanisms described for plunge pools and then evolve to accommodate the plunging flows observed by Venditti et al. (2014).

Plunge pools occur due to pre-existing shifts in bed elevation at waterfalls and overfalls created by either geomorphic or anthropogenic disturbances (Bennett and Alonso, 2005, Pasternack et al., 2007). However, our experiments have shown that scour pools can develop on initially flat channel beds, where only lateral constriction is present. The lateral constriction acts as an obstacle that causes backwater driven deposition upstream of the constriction and erosion downstream of the constriction. The sediment buildup upstream of the constriction creates an elevation difference on the channel bed, which causes flow and sediment to plunge toward the channel bed as they pass through the constriction.

The downward velocity vector is important for controlling erosion rate in bedrock rivers. The vertical component of the particle velocity is used in all abrasion models to determine the energy of particle impact (Sklar and Dietrich, 2004, Lamb et al., 2008, Chatanantavet and Parker, 2009) and impact energy scales directly with erosion rate. The vertical velocity component in abrasion models is derived from saltating particle

velocity, which assumes particles naturally fall towards the bed due to gravity. But the downward velocity vector observed in our experiments works to increase particle's impact energy that results in much higher erosion rates at a canyon entrance, which initiates the pool.

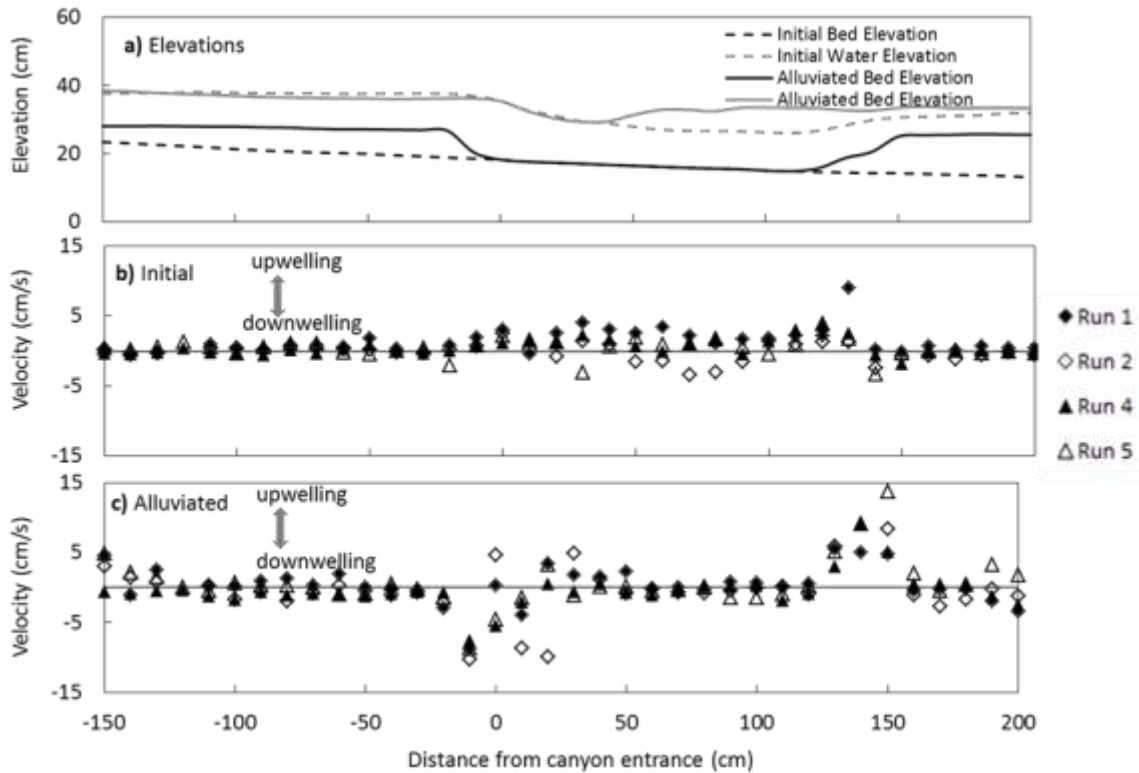


Figure 18. a) Bed and water surface topography during Run 5. Near bed vertical velocity during the b) initial stage and c) alluviated stage

5.4. Relations between velocity, shear stress and erosion patterns

Patterns of near-bed velocity (Figure 15) are strongly correlated with patterns of erosion (Figure 7). There is a spike in near-bed velocity at the canyon entrance that clearly corresponds to the location of the most rapid incision. Another smaller spike in near-bed velocity is present at the secondary pool in the middle of the canyon reach. The decline in near-bed velocity at around 50 cm downstream of the canyon entrance corresponds to a high point between the pools. Flow velocity is directly correlated to erosion rate, as higher velocity means that sediment carried by the flow would impact

the bed with greater energy. Even the mean velocity (Figure 14) is a reasonably good predictor of the erosion pattern.

Counterintuitively, shear stress, regardless of how it is calculated, is decorrelated with erosion rate. The shear stress is higher before the constriction, where the sediment is depositing, and near zero where the erosion rate is highest at the entrance to the first pool. Stress is high over the bed rise between pools, but then declines again at the secondary pool. The reason for this discrepancy is not clear. The use of near bed velocity gradients to calculate shear stress assumes that the near-bed velocity profile is logarithmic, which may not be the case in highly non-uniform flows. However the two point shear stress calculated is correctly representing patterns in the velocity gradient and hence fluid shear (Figure 12). Entering the canyon, the velocity gradient is high (Figure 13). In the canyon reach there is very little difference in velocity with distance above the boundary, resulting in a small gradient and lower fluid shear. The near-bed Reynolds stress appears to mirror the stress from the velocity gradient (Figure 16). This suggests a decoupling of turbulence in the downstream and vertical direction at the canyon entrance due to the highly non-uniform nature of the flow. However, the connection between shear stress and sediment particle motion is tenuous. Particle movements are driven by velocity gradients across particles that cause lift and drag, not necessarily shear stress itself. In uniform flows, shear stress is tightly correlated with near bed velocity as well as instantaneous streamwise and vertical velocity covariance. In highly non-uniform flows, this relation breaks down and near bed velocity becomes a better predictor of sediment particle dynamics (cf. Yager et al., in review). This has important implications for predicting bedrock erosion dynamics which are always driven by highly non-uniform flow. Near-bed velocity appears to be the more relevant predictor of local dynamics than local shear stress.

Chapter 6.

Conclusion

A flume experiment was undertaken to investigate the initiation and evolution of scour pools in bedrock canyons. The channel width was constricted to create a canyon reach with an erodible foam bed, in order to see how lateral constriction influenced flow structure, alluviation patterns, and erosion patterns in a canyon. Lateral constriction can initiate the formation of scour pools within the canyon reach. Sediment deposits upstream of the constriction due to backwater effects create an elevation drop as sediment and flow pass through the constriction. This facilitates flow plunging towards channel bed even when a scour pool is initially absent. The erosion rate within the scour pool is largely dependent on sediment size, transport rate, and location of alluvial cover. In the experiment, scour pools reached equilibrium morphology under constant discharge and sediment supply, due to alluviation within the pool preventing further incision. Lateral erosion within the scour pool was limited, thus resulting in a narrow slot as opposed to a full channel width pool.

Alongstream patterns in near-bed velocity matched erosion patterns, with a spike in velocity where the first scour pool formed, and another smaller spike at the secondary pool. Shear stress is decorrelated with erosion patterns, suggesting near-bed velocity may be a more robust way to calculate erosion rates in highly non-uniform flows. It is still unclear how scour pools expand to full channel width. Further experiments are needed to investigate the lateral expansion of scour pools, with consideration of the lateral secondary recirculation found in bedrock canyons.

References

- Arndt, R.E. a, 1981. Cavitation in Fluid Structures. *Annu. Rev. Fluid Mech.* 13, 273–328.
- Baynes, E.R.C., Attal, M., Niedermann, S., Kirstein, L.A., Dugmore, A.J., Naylor, M., 2015. Erosion during extreme flood events dominates Holocene canyon evolution in northeast Iceland. *Proc. Natl. Acad. Sci.* 112, 2355–2360. doi:10.1073/pnas.1415443112
- Beer, A.R., Turowski, J.M., Kirchner, J.W., 2017. Spatial patterns of erosion in a bedrock gorge. *J. Geophys. Res. Earth Surf.* 122, 191–214. doi:10.1002/2016JF003850
- Bennett, S.J., Alonso, C. V., 2005. Kinematics of flow within headcut scour holes on hillslopes. *Water Resour. Res.* 41, 1–12. doi:10.1029/2004WR003752
- Bollaert, E., Schleiss, A., 2007. Scour of rock due to the impact of plunging high velocity jets Part I: A state-of-the-art review. *J. Hydraul. Res.* 45, 853–858. doi:10.1080/00221686.2007.9521823
- Brownlie, W.R., 1981. Prediction of Flow Depth and Sediment Discharge in Open Channels. Report No. KH-R-43A. W. M. Keck Lab. Hydraul. Water Resour. Calif. Inst. Technol. Pasadena, Calif. 232. doi:10.7907/Z9KP803R
- Chatanantavet, P., Parker, G., 2009. Physically based modeling of bedrock incision by abrasion, plucking, and macroabrasion. *J. Geophys. Res.* 114, F04018. doi:10.1029/2008JF001044
- Cook, K.L., Turowski, J.M., Hovius, N., 2013. A demonstration of the importance of bedload transport for fluvial bedrock erosion and knickpoint propagation. *Earth Surf. Process. Landforms* 38, 683–695. doi:10.1002/esp.3313
- Ervine, D., Falvey, H., W., W., 1999. Pressure fluctuations on plunge pool floors. *J. Hydraul. Res.* 35. doi:10.1080/00221689709498430
- Ferrier, K.L., Huppert, K.L., Perron, J.T., 2013. Climatic control of bedrock river incision. *Nature* 496, 206–209. doi:10.1038/nature11982
- Finnegan, N.J., Sklar, L.S., Fuller, T.K., 2007. Interplay of sediment supply, river incision, and channel morphology revealed by the transient evolution of an experimental bedrock channel. *J. Geophys. Res. Earth Surf.* 112, 1–17. doi:10.1029/2006JF000569
- Fuller, T.K., Gran, K.B., Sklar, L.S., Paola, C., 2016. Lateral erosion in an experimental bedrock channel: The influence of bed roughness on erosion by bed load impacts. *J. Geophys. Res. Earth Surf.* 121, 1–22. doi:10.1002/2015JF003728.Received

- Goodman, R.E., Bray, J.W., 1977. Toppling of rock slopes, in *Rock engineering for foundations and slopes*. New York, Am. Soc. Civ. Eng. 201–234.
- Hancock, G.S., Anderson, R.S., Whipple, K.X., 1998. Beyond Power: Bedrock River Incision Process and Form, in: Tinkler, J.K., Wohl, E.E. (Eds.), *Rivers Over Rock: Fluvial Processes in Bedrock Channels*. AGU, pp. 35–60.
- Howard, A.D., 1994. A detachment-limited model of drainage basin evolution. *Water Resour. Res.* 30, 2261–2285.
- Howard, A.D., Kerby, G., 1983. Channel changes in badlands. *Geol. Soc. Am. Bull.* 94, 739–752.
- Hunt, B., Venditti, J.G., Kwoh, E., 2018. Experiments on the morphological controls of velocity inversions in bedrock canyons. *Earth Surf. Process. Landforms* 43, 654–668. doi:10.1002/esp.4274
- Karlstrom, K.E., Crow, R., Crossey, L.J., Coblenz, D., Wijk, J.W. Van, 2008. Model for tectonically driven incision of the younger than 6 Ma Grand Canyon. *Geology* 36, 835–838. doi:10.1130/G25032A.1
- Lamb, M.P., Dietrich, W.E., 2009. The persistence of waterfalls in fractured rock. *Bull. Geol. Soc. Am.* 121, 1123–1134. doi:10.1130/B26482.1
- Lamb, M.P., Dietrich, W.E., Sklar, L.S., 2008. A model for fluvial bedrock incision by impacting suspended and bed load sediment. *J. Geophys. Res.* 113, F03025. doi:10.1029/2007JF000915
- Lamb, M.P., Finnegan, N.J., Scheingross, J.S., Sklar, L.S., 2015. Geomorphology New insights into the mechanics of fluvial bedrock erosion through flume experiments and theory. *Geomorphology* 244, 33–55. doi:10.1016/j.geomorph.2015.03.003
- Lamb, M.P., Fonstad, M.A., 2010. Rapid formation of a modern bedrock canyon by a single flood event. *Nat. Geosci.* 3, 477–481. doi:10.1038/ngeo894
- Larsen, I.J., Lamb, M.P., 2016. Progressive incision of the Channeled Scablands by outburst floods. *Nature* 538, 229–232. doi:10.1038/nature19817
- Manson, P.J., Arumugam, K., 1985. Free Jet Scour Below Dams and Flip Buckets. *J. Hydraul. Eng.* 111, 220–235.
- Mark, D.M., Church, M., 1977. On the Misuse of Regression in Earth Science. *Math. Geol.* 9, 63–75.

- Martin, V., Fisher, R. S. T., Millar, G. R., Quick, C. M., 2002. ADV Data Analysis for Turbulent Flows: Low Correlation Problem In: Hydraulic measurement and experiment methods 2002, proceedings of the specialty conference July 28–August 1, 2002. ASCE, Estes Park, Colorado, United States
- Nelson, P.A., Seminara, G., 2011. Modeling the evolution of bedrock channel shape with erosion from saltating bed load. *Geophys. Res. Lett.* 38, L17406. doi:10.1029/2011GL048628
- Pasternack, G.B., Ellis, C.R., Marr, J.D., 2007. Jet and hydraulic jump near-bed stresses below a horseshoe waterfall. *Water Resour. Res.* 43, 1–14. doi:10.1029/2006WR005774
- Robinson, K.M., Hanson, G., Cook, K., 2002. Scour below an overfall: Part 1. Investigation. *Trans. ASAE* 45, 949–956.
- Sanders, D., Wischounig, L., Gruber, A., Ostermann, M., 2014. Inner gorge-slot canyon system produced by repeated stream incision (eastern Alps): Significance for development of bedrock canyons. *Geomorphology* 214, 465–484. doi:10.1016/j.geomorph.2014.03.007
- Scheingross, J.S., Brun, F., Lo, D.Y., Omerdin, K., Lamb, M.P., 2014. Experimental evidence for fluvial bedrock incision by suspended and bedload sediment. *Geology* 42, 523–526. doi:10.1130/G35432.1
- Scheingross, J.S., Lamb, M.P., 2017. A mechanistic model of waterfall plunge-pool erosion into bedrock. *J. Geophys. Res. Earth Surf.* 122, 2079–2104. doi:10.1002/2017JF004195
- Shields, A., 1936. Application of Similarity Principles and Turbulence Research to Bed-Load Movement. *Mitt. Preuss. Versuchsanst. Wasserbau Schiffbau* 26, 47.
- Sklar, D.W.E., 2001. Sediment and rock strength controls on river incision into bedrock. *Geology* 29, 1087–1090. doi:10.1130/0091-7613(2001)029<1087:SARSCO>2.0.CO
- Sklar, L.S., Dietrich, W.E., 2004. A mechanistic model for river incision into bedrock by saltating bed load. *Water Resour. Res.* 40, W06301. doi:10.1029/2003WR002496
- Sklar, L.S., Dietrich, W.E., 1998. River Longitudinal Profiles and Bedrock Incision Models: Stream Power and the Influence of Sediment Supply. *Rivers Over Rock Fluv. Process. Bedrock Channels* 107.
- Stark, C.P., 2006. A self-regulating model of bedrock river channel geometry. *Geophys. Res. Lett.* 33, L04402. doi:10.1029/2005GL023193

- Turowski, J.M., Hovius, N., Wilson, A., Horng, M.-J., 2008. Hydraulic geometry, river sediment and the definition of bedrock channels. *Geomorphology* 99, 26–38. doi:10.1016/j.geomorph.2007.10.001
- Venditti, J.G., 2003. Initiation and Development of Sand Dunes in River Channels. Ph.D. Dissertation, University of British Columbia, 291 p.
- Venditti, J.G., Rennie, C.D., Bomhof, J., Bradley, R.W., Little, M., Church, M., 2014. Flow in bedrock canyons. *Nature* 513, 534–537. doi:10.1038/nature13779
- Wahl, T.L., 2000. Analyzing ADV data using WinADV. Build. Partnerships Joint Conf. Water Resour. Eng. Water Resour. Plan. Manag. Minneapolis, Minnesota 1–10. doi:10.1061/40517(2000)300
- Weissel, J.K., Seidl, M.A., 1997. continental margins Influence of rock strength properties on escarpment retreat across passive continental margins. *Geology* 25, 631–634. doi:10.1130/0091-7613(1997)025<0631
- Whipple, K.X., Dibiase, R.A., Crosby, B.T., 2013. Bedrock Rivers, in: *Treatise on Geomorphology*. Elsevier Ltd., pp. 550–573. doi:10.1016/B978-0-12-374739-6.00254-2
- Whipple, K.X., Hancock, G.S., Anderson, R.S., 2000. River incision into bedrock: Mechanics and relative efficacy of plucking, abrasion, and cavitation. *Bull. Geol. Soc. Am.* 112, 490–503. doi:10.1130/0016-7606(2000)112<490:RIIBMA>2.0.CO
- Whiting, P.J., Dietrich, W.E., 1991. Convective accelerations and boundary shear stress over a Channel Bar. *Water Resour. Res.* 27, 783–796. doi:10.1029/91WR00083
- Wobus, C.W., Tucker, G.E., Anderson, R.S., 2006. Self-formed bedrock channels. *Geophys. Res. Lett.* 33, L18408. doi:10.1029/2006GL027182
- Yager, E., Venditti, G. J., Smith, J. H., Schmeeckle, W. M., (in review). The trouble with shear stress. *Geomorphology* (submitted January 5, 2018)
- Yanites, B.J., Tucker, G.E., 2010. Controls and limits on bedrock channel geometry. *J. Geophys. Res. Earth Surf.* 115. doi:10.1029/2009JF001601

Appendix A.

Photograph of flume setup



Figure A1. Photograph of the flume setup during one of the runs. Entrance and exit reaches are alluviated, while the canyon reach is mostly clear.

Appendix B.

Photograph of erosion pattern with sediment

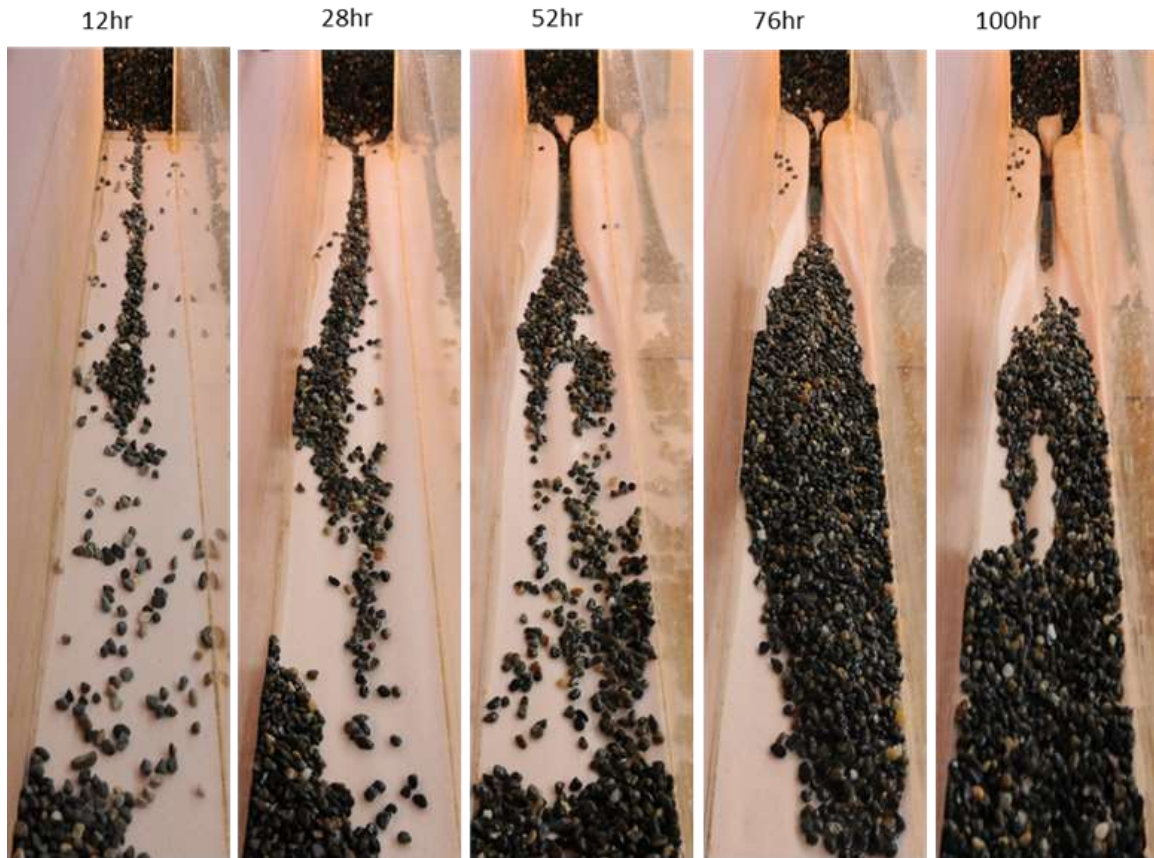


Figure B1. Photographs of erosion pattern from 12 hour to 100 hour for Run 5, taken from same location as photos in Figure 5, but with alluviation in the canyon reach.

Appendix C.

Photograph of short-term alluviation pattern



Figure C1. Consecutive photographs during Run 5 showing short-term alluviation pattern in the canyon reach. The photos are examples of different stages during an alluviation cycle, and not a sequence of one cycle.

Appendix D.

Foam slices showing cross-section of canyon section

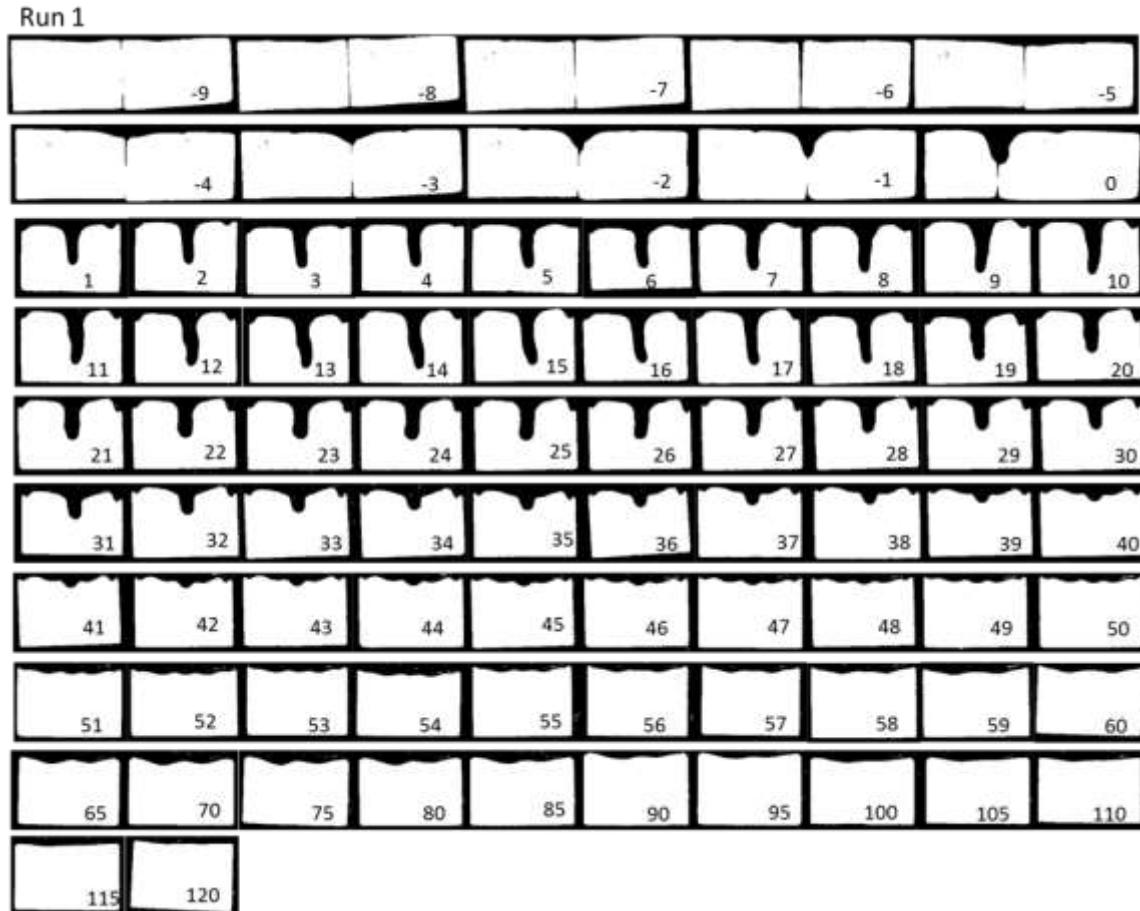


Figure D1. For Run 1, CCPF slices showing cross-section of the canyon section at 1 cm interval for the first 60 cm, and 5 cm interval for the last 60 cm. Numbers on the bottom right indicate position of the slices relative to the canyon entrance, with 0 being at the canyon entrance. Positive numbers are centimeters in the downstream direction and negative numbers are centimeters in the upstream direction.

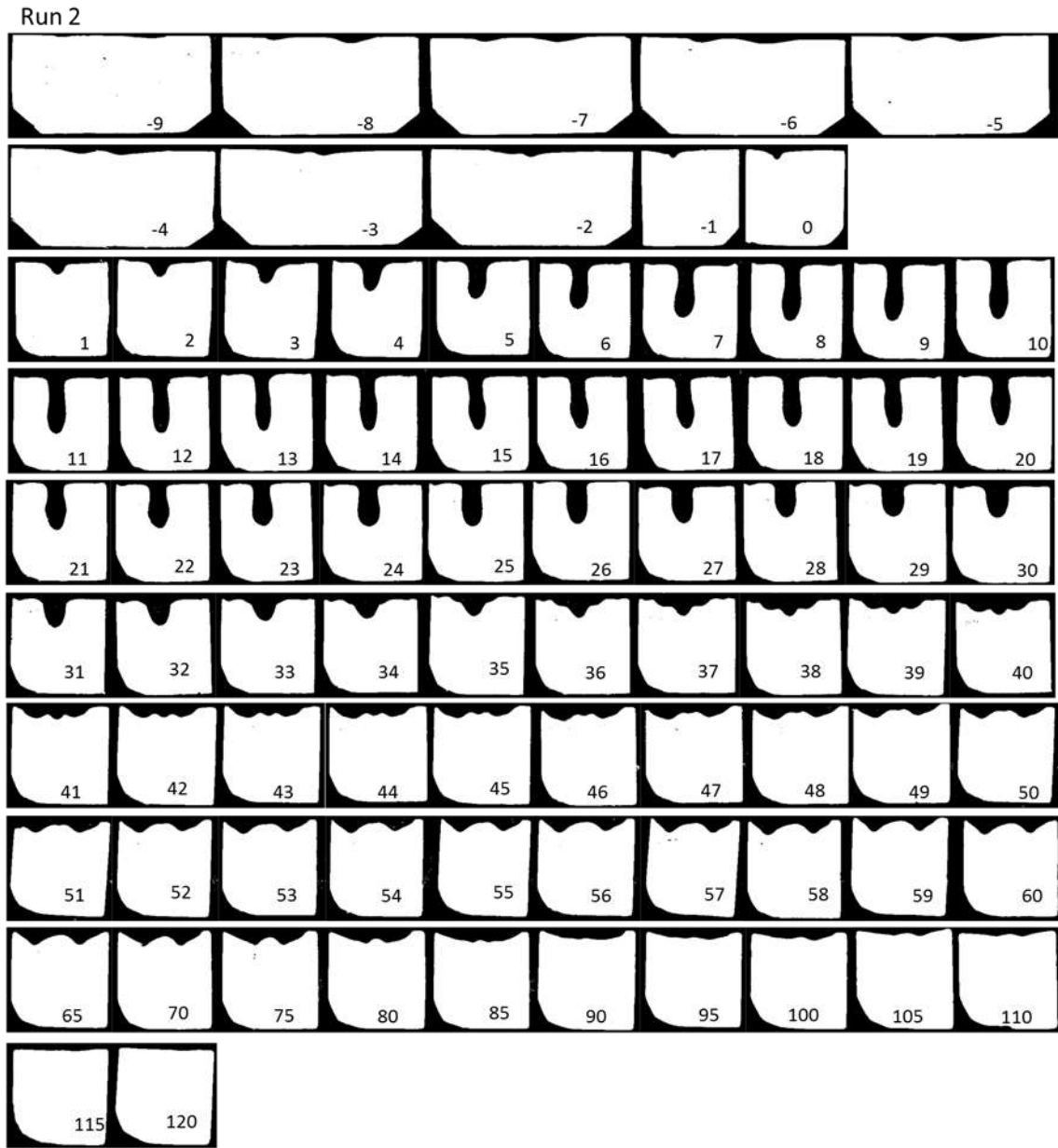


Figure D2. For Run 2, CCPF slices showing cross-section of the canyon section at 1 cm interval for the first 60 cm, and 5 cm interval for the last 60 cm. Numbers on the bottom right indicate position of the slices relative to the canyon entrance, with 0 being at the canyon entrance. Positive numbers are centimeters in the downstream direction and negative numbers are centimeters in the upstream direction.

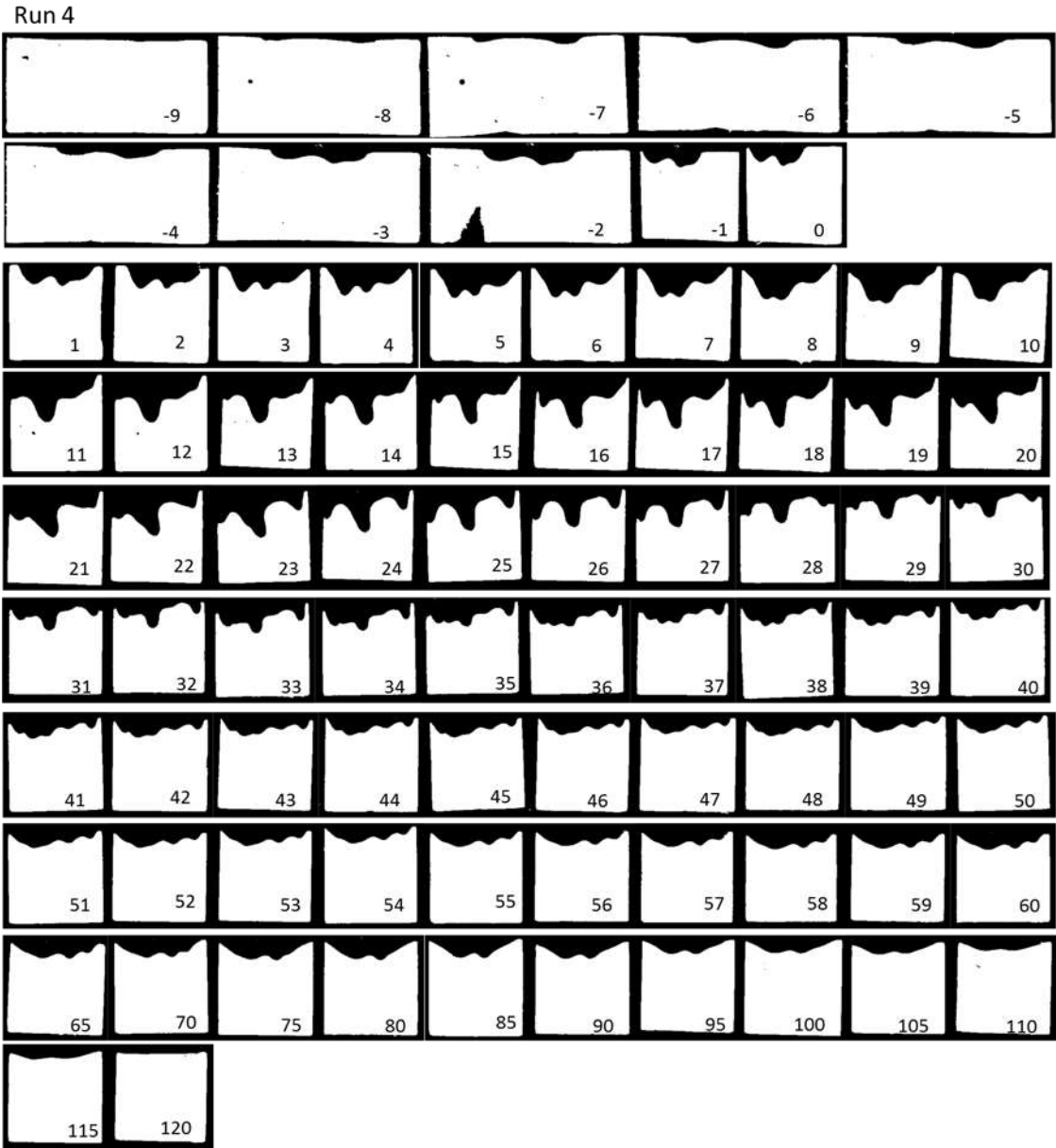


Figure D3. For Run 4, CCPF slices showing cross-section of the canyon section at 1 cm interval for the first 60 cm, and 5 cm interval for the last 60 cm. Numbers on the bottom right indicate position of the slices relative to the canyon entrance, with 0 being at the canyon entrance. Positive numbers are centimeters in the downstream direction and negative numbers are centimeters in the upstream direction.

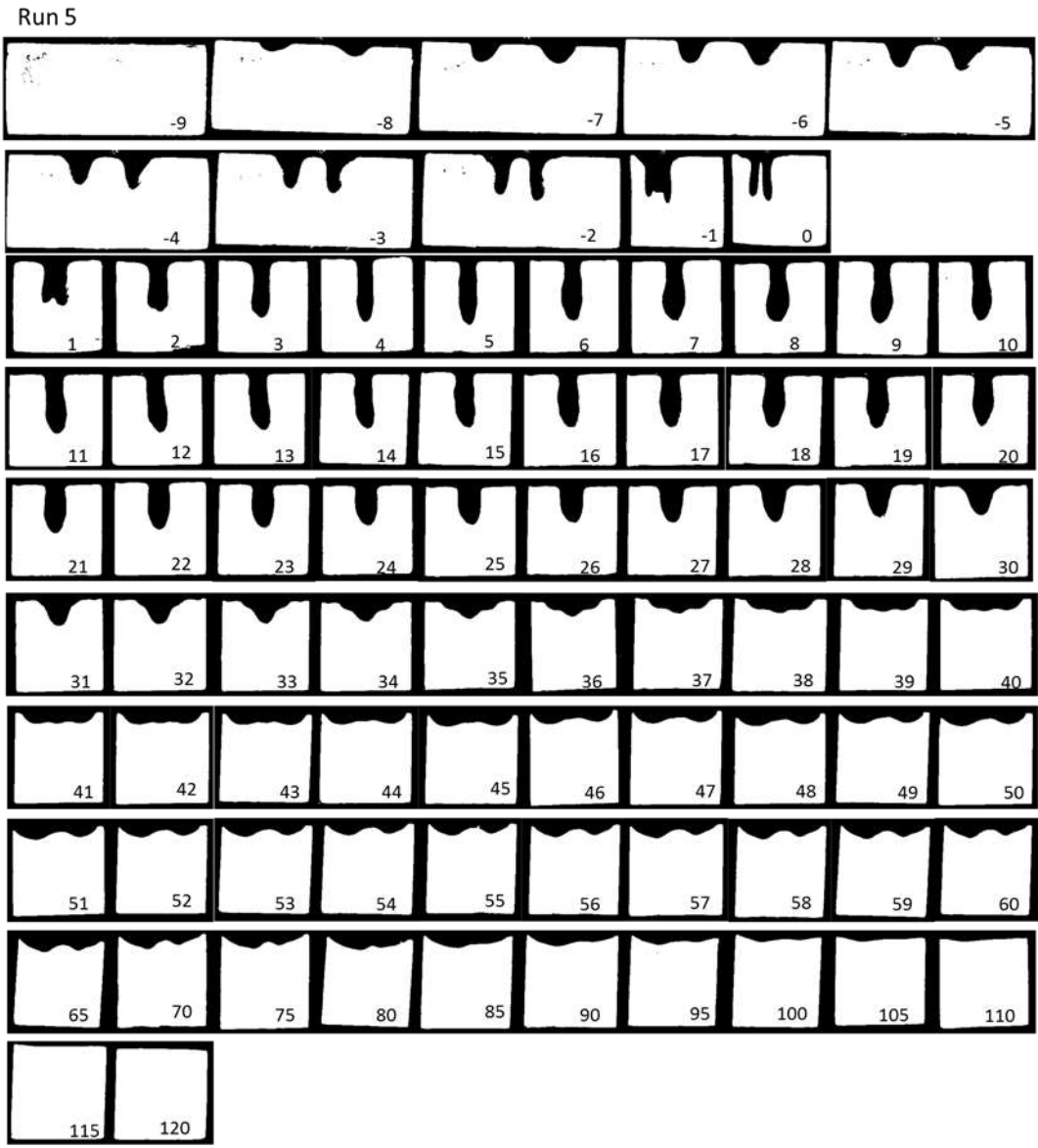


Figure D4. For Run 5, CC PF slices showing cross-section of the canyon section at 1 cm interval for the first 60 cm, and 5 cm interval for the last 60 cm. Numbers on the bottom right indicate position of the slices relative to the canyon entrance, with 0 being at the canyon entrance. Positive numbers are centimeters in the downstream direction and negative numbers are centimeters in the upstream direction. Slice number -1 has a central spire in the center similar to slice number 0, but central spire broken off during cutting process.